

Minimum reflux calculation for multicomponent distillation in multi-feed, multi-product columns: Algorithms and examples

Zheyu Jiang^{*1,3}, Mohit Tawarmalani^{*2}, and Rakesh Agrawal^{†1}

¹Davidson School of Chemical Engineering, Purdue University, West Lafayette, IN 47907

²Mitch Daniels School of Business, Purdue University, West Lafayette, IN 47907

³School of Chemical Engineering, Oklahoma State University, Stillwater, OK 74078

Corresponding authors: zjiang@okstate.edu^{*}, mtawarma@purdue.edu^{*}, agrawalr@purdue.edu[†]

Abstract

In this work, we present the first algorithm for identifying the minimum reboiler vapor duty requirement for a general multi-feed, multi-product (MFMP) distillation column separating ideal multicomponent mixtures. This algorithm incorporates our latest advancement in developing the first shortcut model for MFMP columns. We demonstrate the accuracy and efficiency of this algorithm through case studies. The results obtained from these case studies also provide valuable insights on optimal design of MFMP columns. Many of these insights are against the existing design guidelines and heuristics. For example, placing a colder saturated feed stream above a hotter saturated feed stream sometimes leads to higher energy requirement. Furthermore, decomposing a general MFMP column into individual simple columns may lead to incorrect estimation of the minimum reflux ratio for the MFMP column. Thus, the algorithm presented here offers a fast, accurate, and automated approach to synthesize new, energy-efficient, and cost-effective MFMP columns.

Keywords: Multicomponent distillation, multi-feed and multi-product distillation column, minimum reflux ratio, Underwood method, optimization

1 Introduction

Distillation is a ubiquitous separation technology in the chemical process industries, consuming almost 50% of the energy used by the chemical industries and about 40% by the refining process¹. Assuming that 50% of the CO₂ equivalent release from process heating in chemical manufacturing and 40% in petroleum refining are attributable to distillation, distillation alone would be responsible for 95 million tons of CO₂ release in the U.S. each year². Thus, to decarbonize the U.S. manufacturing sector, it is essential to significantly reduce the energy consumption and carbon footprint of distillation process³.

While binary mixtures can generally be separated using one distillation column, multicomponent mixtures, which are more commonly encountered in industrial separations, require a sequence of columns called a distillation configuration to achieve the desired separation. As the number of components in the feed increases, the total number of possible distillation configurations increases combinatorially⁴. Among these distillation configurations, many of them contain one or more distillation columns with multiple feed streams and/or one or more sidedraw product streams. And it is well-known that these configurations with multi-feed, multi-product (MFMP) columns

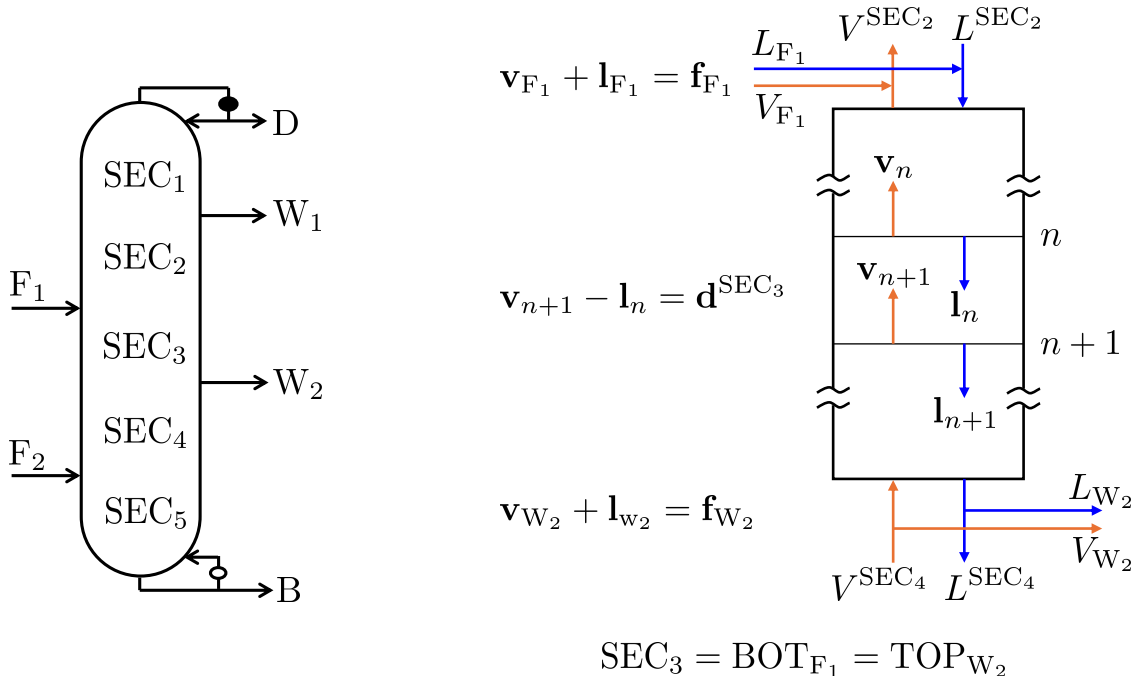


Figure 1: An example MFMP column with three feed streams and two sidedraw product streams and a detailed illustration of liquid and vapor flows within SEC_3 , in which the variables in bold are component flow vectors (e.g., $\mathbf{d}^{\text{sec}_3} = (d_1^{\text{sec}_3}, \dots, d_c^{\text{sec}_3})$ for a c -component system). The column section is numbered from top (1) to bottom ($N_{\text{SEC}} = 5$). The definitions of variables and parameters used here and for the rest of this paper are summarized in Appendices A and B. We follow the convention that \mathbf{v}_{F_j} , \mathbf{l}_{F_j} , and $\mathbf{f}_{F_j} \geq \mathbf{0}$, whereas \mathbf{v}_{W_j} , \mathbf{l}_{W_j} , and $\mathbf{f}_{W_j} \leq \mathbf{0}$.

(see Figure 1 for an example) are generally more energy-efficient to operate than the so called “sharp-split configurations” which do not involve any MFMP column^{5;6}.

MFMP columns can also be derived from conventional one-feed, two-product columns in binary and multicomponent distillation by applying various process intensification techniques⁷⁻⁹, including heat pumps^{10;11}, double and multi-effect¹², intermediate reboilers and condensers¹³, prefractionator arrangement¹⁴, feed preconditioning¹⁵, heat and mass integration¹⁶, and so on. Compared to the original conventional columns, these new MFMP columns not only require significantly less energy from a first-law of thermodynamics perspective, but also have much higher thermodynamic efficiency from a second-law perspective¹⁷, making them more attractive than alternative technologies (e.g., membranes) for a variety of industrial separations^{9;18}. Furthermore, when heat pumps are used in conjunction with other techniques above, the resulting MFMP columns can now be flexibly powered by alternative energy sources (e.g., renewable electricity such as solar and wind). Thus, MFMP columns are becoming increasingly important in the context of industrial decarbonization and net-zero economy, as they can revamp conventional steam-driven distillation systems whose energy primarily comes from fossil fuel combustion².

The minimum reflux ratio of a distillation column is closely related to its energy consumption, capital cost, and operational limit^{19;20}, hence it is a key parameter in distillation design and operation. The naive approach of determining a column’s minimum reflux ratio involves performing exhaustive sensitivity analysis using process simulators, which is a tedious task that often faces convergence issues. As a result, a fast and accurate algorithmic approach to calculate the actual

minimum reflux condition of a general MFMP column is critical for designing new, energy-efficient, and cost-effective multicomponent distillation systems. Ideally, such a method should also have a simple mathematical formulation that can be easily incorporated in a (global) optimization framework for fast and accurate identification of attractive configurations from an enormous configuration search space.

Over the past decades, a number of algorithmic methods have been proposed to determine the minimum reflux ratio of a general MFMP column accurately and efficiently. A comprehensive review of these methods can be found in the first article of this series²¹. However, these methods either rely on several simplifying assumptions, some of which turn out to be too restrictive or even incorrect as we will later demonstrate, or they require rigorous tray-by-tray calculations which are computationally expensive to perform and thus impractical to be implemented for solving complex MFMP columns. To fill the gap between existing methods and what practitioners anticipate, in our previous work²¹, we develop the first shortcut mathematical model to analytically determine the minimum reflux ratio of any general MFMP column entirely based on the assumptions of ideal vapor-liquid equilibrium, constant relative volatility, and constant molar overflow. Our shortcut model is fully generalized as it works for any MFMP column with no particular requirement on feed and/or sidedraw arrangement or product composition specification. Also, the proposed shortcut model does not involve any tray-by-tray calculations. Furthermore, the physical and mathematical properties associated with the shortcut model are explored, from which we successfully derive the mathematical conditions for any general MFMP column operated at minimum reflux. In addition, a relaxation of the constant molar overflow assumption was proposed recently without changing the general mathematical structure of the governing equation²², hence extending the applicability of our shortcut model to real multicomponent systems even further while preserving the mathematical properties and minimum reflux conditions of our shortcut model.

Continuing our previous work²¹, in this article, we introduce an algorithmic method that incorporates the shortcut model developed earlier to efficiently and accurately determine the minimum reboiler vapor duty requirement for a general MFMP column separating a multicomponent mixture. This algorithm can either be used by itself to find the minimum reflux condition for a standalone MFMP column, or can be embedded into a global optimization framework^{6;17;23;24} to simultaneously optimize an entire configuration consisting of one or more MFMP columns. Later, we present three case studies in comparison with rigorous Aspen Plus simulations to illustrate the accuracy and usefulness of our algorithm. Also, we show that results from these case studies could challenge some of the widely-used design heuristics and rules-of-thumb researchers and practitioners have been relying upon. Thus, our shortcut method and the minimum reflux calculation algorithm provide new perspectives on how to accurately model, design, and operate MFMP columns.

2 A Brief Summary of Shortcut Model for MFMP Columns

Before we introduce the minimum reflux calculation algorithm for MFMP columns, we first present a high-level review of the shortcut model we developed earlier²¹ and some of the key results resulting from its derivation, including the mathematical conditions that dictate whether the target separation task can be achieved (with finite or infinite number of stages) in the MFMP column. We encourage readers to refer back to our previous work²¹ for detailed derivations and explanation of these results. We consider a column section, which is separated by either a feed or a product stream, as the smallest module of a MFMP column. The idea is that, by constructing a shortcut model of a column section and exploring its mathematical and physical properties, we can derive

a set of algebraic constraints that must be satisfied for each and every pair of adjacent column sections to maintain connectivity of the (liquid) composition profile between any adjacent sections, hence enforcing the feasibility of separation of the entire MFMP column. In particular, when the target separation can only be achieved by requiring an infinite number of stages (i.e., some column sections have to be pinched), then the corresponding reflux ratio is the minimum reflux ratio of the MFMP column with respect to the target separation goal.

Consider a MFMP column with N_{SEC} number of column sections separated by N_{F} number of feed and N_{W} number of sidedraw streams (note that $N_{\text{SEC}} = N_{\text{F}} + N_{\text{W}} + 1$). Following the nomenclature used in our previous work²¹ and herein summarized in Appendices A and B, for a c -component system, let $\mathcal{C} = \{1, \dots, c\}$ and $\alpha_c > \alpha_{c-1} > \dots > \alpha_1 = 1$ be the relative volatilities with respect to the least volatile component (component 1). Given the feed and product flow rate and composition specifications, we can determine the net material upward flow for component i in column section k , namely $d_i^{\text{SEC}_k}$ (see Figure 1). Then, for a specific section vapor flow V^{SEC_k} , we can solve the following equation²¹ to obtain a total of c roots, $\{\gamma_i^{\text{SEC}_k}\}_{i \in \mathcal{C}}$:

$$\sum_{i=1}^c \frac{\alpha_i d_i^{\text{SEC}_k}}{\alpha_i - \gamma^{\text{SEC}_k}} = V^{\text{SEC}_k}. \quad (1)$$

Suppose $d_c, \dots, d_l > 0$, $d_{l-1}, \dots, d_{h+1} = 0$, and $d_h, \dots, d_1 < 0$ for some $1 \leq h < l \leq c$ in a column section. In other words, more volatile components c, \dots, l have net material upward flows, intermediately volatile components $l-1, \dots, h+1$ have net zero material flows, and less volatile components $h, \dots, 1$ have net material downward flows. It can be verified that all c roots lie in the following intervals:

$$\begin{aligned} \gamma_i^{\text{SEC}_k} &\in (\alpha_i, \alpha_{i+1}) && \text{for } i \in \{1, \dots, h\} \\ \gamma_i^{\text{SEC}_k} &= \alpha_i && \text{for } i \in \{h+1, \dots, l-1\} \\ \gamma_i^{\text{SEC}_k} &\in (\alpha_{i-1}, \alpha_i) && \text{for } i \in \{l, \dots, c\}. \end{aligned} \quad (2)$$

As for the edge cases, when $l = h+1$, meaning that there are no intermediate components with net zero material flows, there are two roots in the interval $(\alpha_h, \alpha_l) = (\alpha_h, \alpha_{h+1})$ and exactly one root in each of the remaining $c-1$ relative volatility intervals (see Figure 2). It turns out that the pinch root $\gamma_p^{\text{SEC}_k}$ (the subscript p stands for ‘‘pinch’’ and its value corresponds to the pinch index), which determines the actual pinch zone composition in SEC_k , actually lies in (α_h, α_l) . That is, the pinch root lies in relative volatility interval where the sign change in d_i occurs²¹.

For the second edge case, when $h = 0$, meaning that all components have non-negative net material upward flow in SEC_k , we have $\gamma_i^{\text{SEC}_k} = \alpha_i$ for $i \in \{1, \dots, l-1\}$ and $\gamma_i^{\text{SEC}_k} \in (\alpha_{i-1}, \alpha_i)$ for $i \in \{l, \dots, c\}$. In this case, the pinch root $\gamma_p^{\text{SEC}_k} = \gamma_l^{\text{SEC}_k} \in (\alpha_{l-1}, \alpha_l)$. Additionally, if $l = 1$, meaning that all components have net material upward flow in the column section, we have $\gamma_i^{\text{SEC}_k} \in (\alpha_{i-1}, \alpha_i)$ for $i \in \mathcal{C}$, where α_0 is defined as 0. And the pinch root $\gamma_p^{\text{SEC}_k} = \gamma_1^{\text{SEC}_k} \in (\alpha_0, \alpha_1)$.

Lastly, when $l = c+1$, meaning that all components have non-positive net material upward flow in SEC_k , we have $\gamma_i^{\text{SEC}_k} \in (\alpha_i, \alpha_{i+1})$ for $i \in \{1, \dots, h\}$ and $\gamma_i^{\text{SEC}_k} = \alpha_i$ for $i \in \{h+1, \dots, c\}$. In this case, the pinch root $\gamma_p^{\text{SEC}_k} = \gamma_h^{\text{SEC}_k} \in (\alpha_h, \alpha_{h+1})$. Additionally, if $h = c$, meaning that all components have net material downward flow in the column section, we have $\gamma_i^{\text{SEC}_k} \in (\alpha_i, \alpha_{i+1})$ for $i \in \mathcal{C}$. Here, we denote $\alpha_{c+1} = \alpha_c + \delta$, where δ is set to be a sufficient large number. And the pinch root $\gamma_p^{\text{SEC}_k} = \gamma_c^{\text{SEC}_k} \in (\alpha_c, \alpha_{c+1})$.

Now that we have reviewed the key results of our shortcut model, in the next section, we will

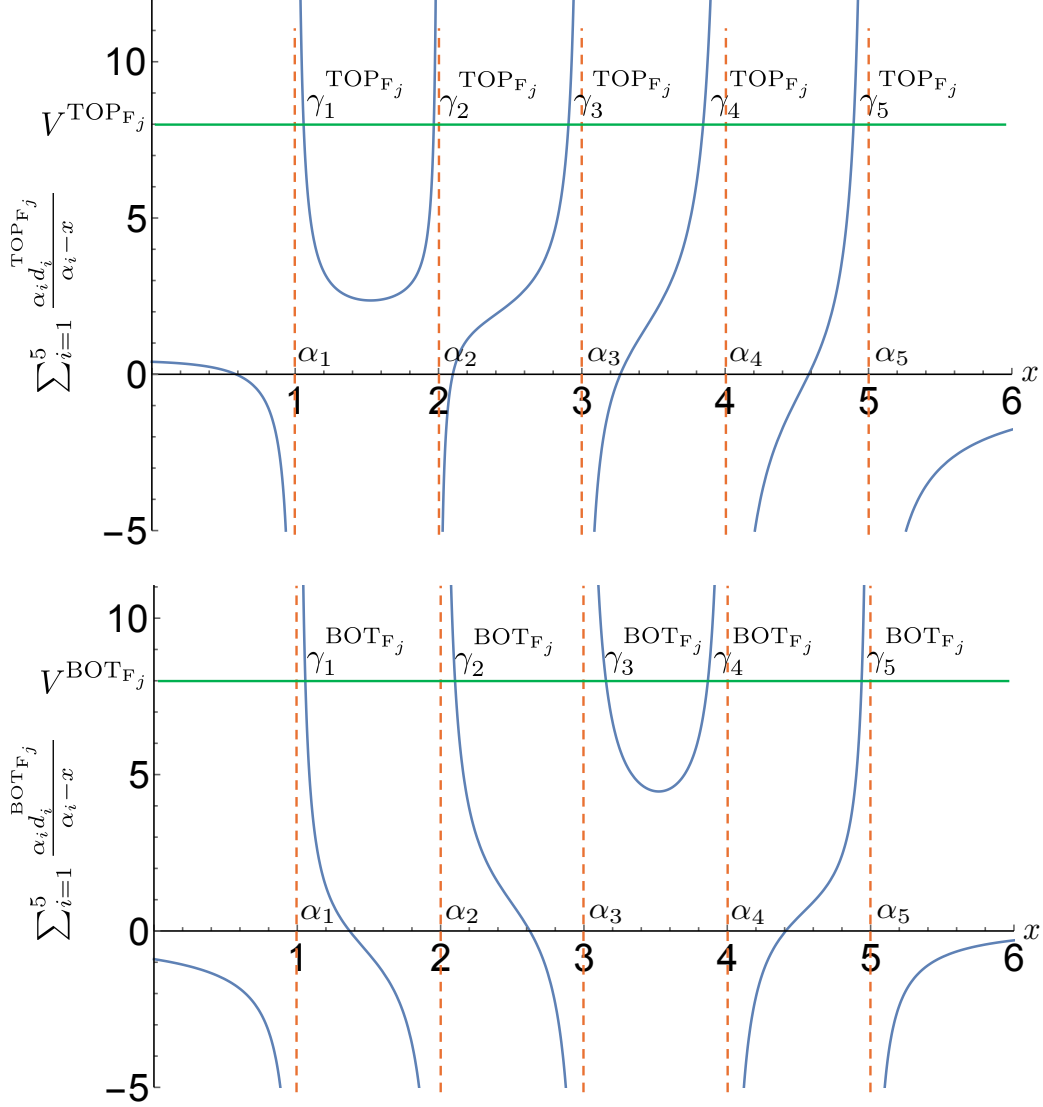


Figure 2: Roots of Equation (1) for a five-component illustrative example where $(d_1, d_2, d_3, d_4, d_5) = (-0.4, 0.1, 0.2, 0.3, 0.2)$ for section TOP_{F_j} , $(d_1, d_2, d_3, d_4, d_5) = (-0.4, 0.1, 0.2, 0.3, 0.2)$ for feed TOP_{F_j} , and $(d_1, d_2, d_3, d_4, d_5) = (-0.5, -0.4, -0.3, 0.2, 0.1)$ for section BOT_{F_j} . The relative volatilities are $(\alpha_1, \alpha_2, \alpha_3, \alpha_4, \alpha_5) = (1, 2, 3, 4, 5)$. The section vapor flow V is set to be 8 and F_j is a saturated liquid. In this case, the pinch roots $\gamma_p^{\text{TOP}_{F_j}} \in (\alpha_1, \alpha_2)$ and $\gamma_p^{\text{BOT}_{F_j}} \in (\alpha_3, \alpha_4)$.

derive the algorithmic formulation to determine the minimum reflux ratio or minimum reboiler vapor duty for a general MFMP column.

3 Minimum Reflux Condition Formulation for MFMP Columns

Recall that for c -component system, the domain of $\gamma_i^{\text{SEC}_k}$ roots to Equation (1) can be split into $c + 1$ distinct intervals: $(0, \alpha_1)$, (α_1, α_2) , \dots , (α_{c-1}, α_c) , and $(\alpha_c, \alpha_c + \delta)$, where δ is a sufficiently large positive number. The pinch root $\gamma_p^{\text{SEC}_k}$ for SEC_k must lie in one of these $c + 1$ intervals. Thus,

we may define a set of binary variables $\{\mu_i^{\text{SEC}_k} \in \{0, 1\}\}_{i=1}^{c+1}$, where $\mu_i^{\text{SEC}_k} = 1$ when the pinch root $\gamma_p^{\text{SEC}_k} \in (\alpha_{i-1}, \alpha_i)$, and is 0 otherwise. Here, we denote $\alpha_0 = 0$. This way, the pinch root must satisfy the following constraints:

$$\begin{aligned} \sum_{i=1}^{c+1} \alpha_{i-1} \mu_i^{\text{SEC}_k} &\leq \gamma_p^{\text{SEC}_k} \leq \sum_{i=1}^{c+1} \alpha_i \mu_i^{\text{SEC}_k} \\ \sum_{i=1}^{c+1} \mu_i^{\text{SEC}_k} &= 1 \end{aligned} \quad \forall k = 1, \dots, N_{\text{SEC}}. \quad (3)$$

When two adjacent column sections are separated by a feed stream F_j ($j = 1, \dots, N_F$), we denote the section above F_j as TOP_{F_j} and the one below as BOT_{F_j} (see Figure 1). Since $d_i^{\text{TOP}_{F_j}} - d_i^{\text{BOT}_{F_j}} = f_{i,F_j} \geq 0$, we have $d_i^{\text{TOP}_{F_j}} \geq d_i^{\text{BOT}_{F_j}}$ for $i \in \mathcal{C}$, indicating that the pinch index for TOP_{F_j} would be at most the same as the pinch index for BOT_{F_j} , hence satisfying $p^{\text{TOP}_{F_j}} \leq p^{\text{BOT}_{F_j}}$, or:

$$\sum_{i=1}^{c+1} i \mu_{i,\text{BOT}_{F_j}} \geq \sum_{i=1}^{c+1} i \mu_{i,\text{TOP}_{F_j}} \quad \forall j = 1, \dots, N_F. \quad (4)$$

We define an index set \mathcal{I}_{F_j} storing all indices of intervals ranging from $\max\{2, \sum_{i=1}^{c+1} i \mu_{i,\text{TOP}_{F_j}}\}$ to $\min\{c, \sum_{i=1}^{c+1} i \mu_{i,\text{BOT}_{F_j}}\}$ (i.e., considering intervals within α_1 and α_c and excluding the two intervals (α_0, α_1) and (α_c, α_{c+1})). To better characterize \mathcal{I}_{F_j} , we define a new set of binary variables $\{K_i^{\text{SEC}_k} \in \{0, 1\}\}_{i=1}^{c+1}$ for column section k where:

$$K_i^{\text{SEC}_k} = \sum_{m=1}^i \mu_m^{\text{SEC}_k} \quad \forall i = 1, \dots, c+1; k = 1, \dots, N_{\text{SEC}}. \quad (5)$$

Clearly, $K_i^{\text{SEC}_k} = 0$ if and only if $\mu_1^{\text{SEC}_k}, \dots, \mu_i^{\text{SEC}_k}$ are all equal to 0. And $K_i^{\text{SEC}_k}$ changes from 0 to 1 at index i where $\mu_i^{\text{SEC}_k} = 1$ (i.e., $\gamma_p^{\text{SEC}_k} \in (\alpha_{i-1}, \alpha_i)$) and then stays at 1 for indices greater than i . Knowing this, it can be verified that \mathcal{I}_{F_j} can be equivalently expressed as:

$$\mathcal{I}_{F_j} = \{i \in \mathcal{C} | K_i^{\text{TOP}_{F_j}} - K_{i-1}^{\text{BOT}_{F_j}} = 1\} \quad \forall j = 1, \dots, N_F. \quad (6)$$

For example, consider the same five-component system whose root profiles for TOP_{F_j} and BOT_{F_j} are shown in Figure 2. Correspondingly, the relationship between $m\mu_i$ and K_i variables for this illustrative example is shown in Figure 3. Following Equation (6), we have $\mathcal{I}_{F_j} = \{2, 3, 4\}$.

With this, one of the key results obtained in our previous work²¹ is that, the feasibility of the target separation requires the following constraint to be satisfied in sections TOP_{F_j} and BOT_{F_j} for every $i \in \mathcal{I}_{F_j}$:

$$\gamma_i^{\text{TOP}_{F_j}} \geq \rho_{i-1,F_j} \geq \gamma_{i-1}^{\text{BOT}_{F_j}} \quad \forall i \in \mathcal{I}_{F_j}; j = 1, \dots, N_F \quad (7)$$

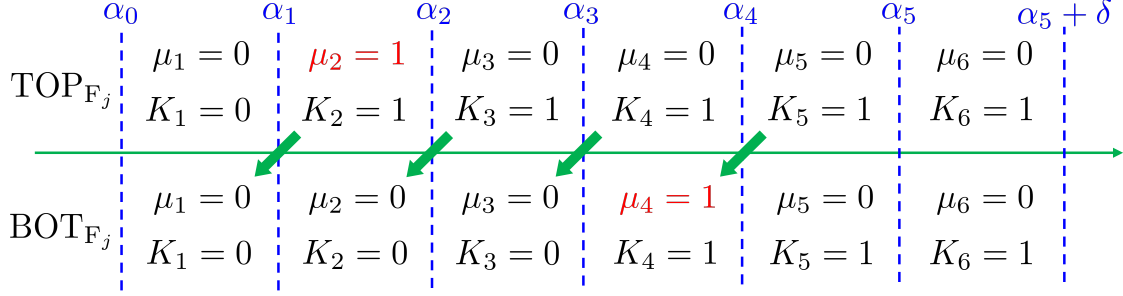


Figure 3: The relationship between μ_i and K_i variables for the example illustrated in Figure 2. The green arrows show how the (binary) coefficients in Equation (9) are constructed. For this example, $K_2^{\text{TOP}_{F_j}} - K_1^{\text{BOT}_{F_j}} = K_3^{\text{TOP}_{F_j}} - K_2^{\text{BOT}_{F_j}} = K_4^{\text{TOP}_{F_j}} - K_3^{\text{BOT}_{F_j}} = 1$. Therefore, $\mathcal{I}_{F_j} = \{2, 3, 4\}$ according to Equation (6).

where $\{\rho_{i-1, F_j}\}_{i \in \mathcal{I}_{F_j}}$ satisfy:

$$\sum_{m=1}^c \frac{\alpha_m l_{m, F_j}}{\alpha_m - \rho_{i-1, F_j}} = 0 \quad \text{or} \quad \sum_{m=1}^c \frac{\alpha_m f_{m, F_j}}{\alpha_m - \rho_{i-1, F_j}} = V_{F_j} \quad j = 1, \dots, N_F, \quad (8)$$

where $\rho_{i-1, F_j} \in (\alpha_{i-1}, \alpha_i)$. Here, $l_{m, F_j} \geq 0$, $f_{m, F_j} \geq 0$, and $V_{F_j} \geq 0$ correspond to the flow rate of component m in the liquid portion of F_j , the feed flow rate of component m , and the total vapor flow rate of the feed, respectively. When F_j is in saturated vapor state, then l_{m, F_j} represents the hypothetical liquid feed flow that is in thermodynamic equilibrium with the vapor feed²¹:

$$l_{m, F_j} = \frac{\frac{v_{m, F_j}}{\alpha_m}}{\sum_{k=1}^c \frac{v_{k, F_j}}{\alpha_k}} \quad \forall m \in \mathcal{C}.$$

To implement Equation (7) algorithmically, we leverage the fact that $K_i^{\text{TOP}_{F_j}} - K_{i-1}^{\text{BOT}_{F_j}}$ is itself a binary variable indicating whether index $i \in \mathcal{I}_{F_j}$ or not. Thus, Equation (7) can be rewritten as:

$$\begin{aligned} (K_i^{\text{TOP}_{F_j}} - K_{i-1}^{\text{BOT}_{F_j}})(\gamma_i^{\text{TOP}_{F_j}} - \rho_{i-1, F_j}) &\geq 0 \\ (K_i^{\text{TOP}_{F_j}} - K_{i-1}^{\text{BOT}_{F_j}})(\rho_{i-1, F_j} - \gamma_{i-1}^{\text{BOT}_{F_j}}) &\geq 0 \end{aligned} \quad \forall i \in \mathcal{C} \setminus \{1\}; j = 1, \dots, N_F. \quad (9)$$

When two adjacent column sections are connected by a sidedraw stream W_j ($j = 1, \dots, N_W$), we denote the section above W_j as TOP_{W_j} and the one below as BOT_{W_j} . Since $d_i^{\text{TOP}_{W_j}} - d_i^{\text{BOT}_{W_j}} = f_{i, W_j} \leq 0$, we have $d_i^{\text{TOP}_{W_j}} \leq d_i^{\text{BOT}_{W_j}}$ for $i \in \mathcal{C}$, indicating that the pinch index for section TOP_{W_j} would be at least the same as the pinch index for section BOT_{W_j} , hence satisfying $p^{\text{TOP}_{W_j}} \geq p^{\text{BOT}_{W_j}}$. Thus, we have:

$$\sum_{i=1}^{c+1} i \mu_{i, \text{BOT}_{W_j}} \leq \sum_{i=1}^{c+1} i \mu_{i, \text{TOP}_{W_j}} \quad \forall j = 1, \dots, N_W. \quad (10)$$

Similar to \mathcal{I}_{F_j} for feed stream F_j , we define an index set \mathcal{I}_{W_j} storing all indices of intervals ranging from $\max\{2, \sum_{i=1}^{c+1} i \mu_{i, \text{BOT}_{W_j}}\}$ to $\min\{c, \sum_{i=1}^{c+1} i \mu_{i, \text{TOP}_{W_j}}\}$. Furthermore, \mathcal{I}_{W_j} can also be

redefined as:

$$\mathcal{I}_{W_j} = \{i \in \mathcal{C} | K_i^{\text{BOT}_{W_j}} - K_{i-1}^{\text{TOP}_{W_j}} = 1\} \quad \forall j = 1, \dots, N_W. \quad (11)$$

The feasibility of separation requires the following constraint to hold for TOP_{W_j} and BOT_{W_j} for every $i \in \mathcal{I}_{W_j}$ ²¹:

$$\gamma_{i-1}^{\text{TOP}_{W_j}} \leq \rho_{i-1, W_j} \leq \gamma_i^{\text{BOT}_{W_j}} \quad \forall i \in \mathcal{I}_{W_j}; j = 1, \dots, N_W, \quad (12)$$

where $\{\rho_{i-1, W_j}\}_{i \in \mathcal{I}_{W_j}}$ satisfy Equation (13) below:

$$\sum_{m=1}^c \frac{\alpha_m l_{m, W_j}}{\alpha_m - \rho_{i-1, W_j}} = 0, \quad \text{or} \quad \sum_{m=1}^c \frac{\alpha_m f_{m, W_j}}{\alpha_m - \rho_{i-1, W_j}} = V_{W_j} \quad j = 1, \dots, N_W, \quad (13)$$

where $\rho_{i-1, W_j} \in (\alpha_{i-1}, \alpha_i)$. Here, $l_{m, W_j} \leq 0$, $f_{m, W_j} \leq 0$, and $V_{W_j} \leq 0$ correspond to the flow rate of component m in the liquid portion of the sidedraw stream, the sidedraw flow rate of component m , and the total vapor flow rate of the sidedraw, respectively. When W_j is in saturated vapor state, then l_{m, W_j} represents the hypothetical liquid sidedraw flow that is in thermodynamic equilibrium with the vapor sidedraw²¹:

$$l_{m, W_j} = \frac{\frac{v_{m, W_j}}{\alpha_m}}{\sum_{k=1}^c \frac{v_{k, W_j}}{\alpha_k}} \quad \forall m \in \mathcal{C}.$$

Similar to how we reformulate Equation (7) for F_j , we can rewrite Equation (12) as:

$$\begin{aligned} (K_i^{\text{BOT}_{W_j}} - K_{i-1}^{\text{TOP}_{W_j}})(\gamma_i^{\text{BOT}_{W_j}} - \rho_{i-1, W_j}) &\geq 0 \\ (K_i^{\text{BOT}_{W_j}} - K_{i-1}^{\text{TOP}_{W_j}})(\rho_{i-1, W_j} - \gamma_{i-1}^{\text{TOP}_{W_j}}) &\geq 0 \end{aligned} \quad \forall i \in \mathcal{C} \setminus \{1\}; j = 1, \dots, N_W. \quad (14)$$

Furthermore, as illustrated in Figure 1, a unique feature about a sidedraw stream is that the sidedraw's liquid (resp. vapor) composition must lie on the liquid (resp. vapor) composition profile, whereas a feed stream's liquid (resp. vapor) composition may or may not lie on the liquid (resp. vapor) composition profile. The condition that sidedraw composition must belong to the composition profile yields to the following set of constraints:

$$\begin{aligned} K_i^{\text{TOP}_{W_j}}(\gamma_i^{\text{TOP}_{W_j}} - \rho_{i-1, W_j}) &\geq 0 \quad \forall i \in \mathcal{C} \setminus \{1\}; \\ K_i^{\text{BOT}_{W_j}}(\gamma_i^{\text{BOT}_{W_j}} - \rho_{i-1, W_j}) &\geq 0 \quad \forall i \in \mathcal{C} \setminus \{1\}; \\ (1 - K_i^{\text{TOP}_{W_j}})(\gamma_i^{\text{TOP}_{W_j}} - \rho_{i, W_j}) &\leq 0 \quad \forall i \in \mathcal{C}; \\ (1 - K_i^{\text{BOT}_{W_j}})(\gamma_i^{\text{BOT}_{W_j}} - \rho_{i, W_j}) &\leq 0 \quad \forall i \in \mathcal{C}; \end{aligned} \quad \forall j = 1, \dots, N_W. \quad (15)$$

4 Implementation of Minimum Reflux Calculation Algorithm

When implementing the algorithm developed in Section 3, there are two approaches to consider. The first approach is to implement Equations (3), (4), (5), (9), (14) and (15) in an optimization framework as constraints, along with the mathematical formulations of the shortcut model developed in our earlier work²¹, which includes Equations (1), (8), (13), and more. The resulting formulation is a mixed-integer nonlinear program (MINLP), which can be solved to global opti-

mality using global solvers such as BARON²⁵. We pursue this approach when only the purity or recovery of the key components in product streams are specified. In this case, the MINLP will determine the optimal distribution of other components in the product streams such that the reflux ratio or reboiler vapor duty requirement is minimized. To illustrate how this approach works, in Section 5.3, we present this formulation for an quaternary separation example in a two-feed, one-sidedraw column.

input : \mathcal{C} , N_F , N_W , N_{SEC} , $\{f_{i,F_j}\}_{j=1}^{N_F}$, $\{l_{i,F_j}\}_{j=1}^{N_F}$, $\{f_{i,W_j}\}_{j=1}^{N_W}$, $\{l_{i,W_j}\}_{j=1}^{N_W}$, $d_i^{SEC_1}$ for every component $i \in \mathcal{C}$
output: minimum reboiler vapor duty $V_{reb,min}$
initialize: An empty list $\{V_{reb}\}$ storing candidate minimum reboiler vapor duty values
begin
 Calculate $\{d_i^{SEC_k}\}_{i \in \mathcal{C}; k=2, \dots, N_{SEC}}$ from inter-column section material balances (Equation (29) of Jiang et al.²¹);
 Determine pinch root $\{\gamma_p^{SEC_k}\}_{k=1, \dots, N_{SEC}}$ locations from Equation (2) and other edge cases, then obtain $\{\mu_i^{SEC_k}\}_{i \in \mathcal{C}, k=1, \dots, N_{SEC}}$ and $\{K_i^{SEC_k}\}_{i \in \mathcal{C}, k=1, \dots, N_{SEC}}$;
 Determine index sets $\{\mathcal{I}_{F_j}\}_{j=1}^{N_F}$ and $\{\mathcal{I}_{W_j}\}_{j=1}^{N_W}$ from Equations (6) and (11);
 Solve Equations (8) and (13) to obtain $\{\rho_{i-1,F_j}\}_{i \in \mathcal{C} \setminus \{1\}; j=1, \dots, N_F}$ and $\{\rho_{i-1,W_j}\}_{i \in \mathcal{C} \setminus \{1\}; j=1, \dots, N_W}$ roots, respectively;
 for $j \leftarrow 1$ **to** N_W **do**
 Add $V_{reb,W_j} = \text{sidedrawFeasible}(j, \{K_i^{TOP_{W_j}}\}_i)$ into the list $\{V_{reb}\}$ and continue;
 if $\mathcal{I}_{W_j} = \emptyset$ **then** Skip and go to the next j **else** Continue;
 for $i \in \mathcal{I}_{W_j}$ **do**
 Substitute $\gamma_{i-1}^{TOP_{W_j}} \leftarrow \rho_{i-1,W_j}$ into Equation (1) to obtain $V^{TOP_{W_j}}$;
 Add $V_{reb,W_j} = \text{getVreb}(TOP_{W_j}, V^{TOP_{W_j}})$ into the list $\{V_{reb}\}$;
 end
 end
 for $j \leftarrow 1$ **to** N_F **do**
 if $\mathcal{I}_{F_j} = \emptyset$ **then** Skip and go to the next j **else** Continue;
 for $i \in \mathcal{I}_{F_j}$ **do**
 Substitute $\gamma_i^{TOP_{F_j}} \leftarrow \rho_{i-1,F_j}$ into Equation (1) to obtain $V^{TOP_{F_j}}$;
 Add $V_{reb,F_j} = \text{getVreb}(TOP_{F_j}, V^{TOP_{F_j}})$ into the list $\{V_{reb}\}$;
 end
 end
 $V_{reb,min} = \min\{V_{reb}\}$
end

Algorithm 1: Vrebmin: Algorithm for determining the minimum reboiler vapor duty requirement of a MFMP column knowing the flow rates and compositions of feed and product streams. The minimum reflux ratio R_{min} can be readily calculated from vapor balances once $V_{reb,min}$ is obtained, since all feed and product flow rates are specified.

The second approach deals with many practical applications in which the product distributions of the MFMP column have already been adequately specified. In this case, the search for minimum reflux ratio of the MFMP column becomes a fully algorithmic procedure that does not require solving an optimization problem. This is because the net material upward flows $\{d_i^{SEC_k}\}_{i \in \mathcal{C}, k=1, \dots, N_{SEC}}$

input : column section s and its section vapor flow V^{SEC_s}
output: candidate reboiler vapor duty value

```

begin
  for  $k \leftarrow s - 1$  to 1 do
    Calculate  $V^{\text{SEC}_k}$  from  $V^{\text{SEC}_{k+1}}$  via vapor balances;
    Determine  $\{\gamma_r^{\text{SEC}_k}\}_{r \in \mathcal{C}}$  from Equation (1) using  $V^{\text{SEC}_k}$ ;
    if the feasibility constraints (Equations (7), (12), (15)) associated with  $\text{SEC}_k$  are
       satisfied then Continue else return null;
    end
  for  $k \leftarrow s + 1$  to  $N_{\text{SEC}}$  do
    Calculate  $V^{\text{SEC}_k}$  from  $V^{\text{SEC}_{k-1}}$  via vapor balances;
    Determine  $\{\gamma_r^{\text{SEC}_k}\}_{r \in \mathcal{C}}$  from Equation (1) using  $V^{\text{SEC}_k}$ ;
    if the feasibility constraints (Equations (7), (12), (15)) associated with  $\text{SEC}_k$  are
       satisfied then Continue else return null;
    end
  end
  return  $V^{\text{SEC}_{N_{\text{SEC}}}}$ .
end

```

Algorithm 2: getVreb: Algorithm for checking feasibility of separation and returning the candidate reboiler vapor duty value.

input : sidedraw stream index j and index set $\{K_i^{\text{TOP}_{W_j}}\}_i$
output: candidate reboiler vapor duty value
initialize: An empty list $\{V_{\text{reb},W_j}\}$ storing candidate minimum reboiler vapor duty values

```

begin
  for  $m \leftarrow 1$  to  $c$  do
    if  $K_m^{\text{TOP}_{W_j}} = 0$  then
      Substitute  $\gamma_m^{\text{TOP}_{W_j}} \leftarrow \rho_{m,W_j}$  into Equation (1) to obtain  $V^{\text{TOP}_{W_j}}$ ; Add
         $V_{\text{reb},m} = \text{getVreb}(\text{TOP}_{W_j}, V^{\text{TOP}_{W_j}})$  into the list  $\{V_{\text{reb},W_j}\}$ ;
    else
      Substitute  $\gamma_m^{\text{TOP}_{W_j}} \leftarrow \rho_{m-1,W_j}$  into Equation (1) to obtain  $V^{\text{TOP}_{W_j}}$ ; Add
         $V_{\text{reb},m} = \text{getVreb}(\text{TOP}_{W_j}, V^{\text{TOP}_{W_j}})$  into the list  $\{V_{\text{reb},W_j}\}$ ;
    end
  end
  return  $V^{\text{SEC}_{N_{\text{SEC}}}} \leftarrow \min\{V_{\text{reb},W_j}\}$ .
end

```

Algorithm 3: sidedrawFeasible: Algorithm for returning candidate reboiler vapor duty value assuming that the minimum reflux is “controlled” by a sidedraw.

can be readily obtained from mass balances, making the determination of pinch root location (hence \mathcal{I}_F and \mathcal{I}_W sets) completely deterministic for every feed and sidedraw stream. Therefore, we can run a simple algorithmic procedure, as shown in Algorithms 1 through 3, to identify the true minimum reboiler vapor duty requirement (or equivalently the minimum reflux ratio since all product flows are fixed). Specifically, as discussed in detail in our previous work²¹, at minimum reflux condition, one of the feed or sidedraw streams essentially “controls” the separation. Accordingly, while the feasibility constraints (Equation (7) or (12)) associated with feed and/or sidedraw streams continue to hold, the feasibility constraints associated with the controlling feed or sidedraw stream will become binding (i.e., satisfied as equalities). Thus, the idea behind Algorithms 1 through 3 is to scrutinize all feed and sidedraw streams, assuming that each of them might be “controlling” the separation at minimum reflux, and determine whether feasibility constraints are met for the rest of feed and sidedraw streams. Overall, the true reboiler vapor duty (resp. minimum minimum reflux ratio) corresponds to the lowest reboiler vapor duty (resp. lowest reflux ratio) at which all feasibility constraints are satisfied.

5 Case Studies

In this section, we examine a few ternary and quaternary separation examples that will illustrate the accuracy and effectiveness of our minimum reflux calculation methods while providing valuable insights of the minimum reflux behavior of a MFMP column for the first time.

5.1 Example 1: Two-Feed Distillation Column

In the first example, we examine a two-feed distillation column shown in Figure 4 separating a ternary mixture of n-hexane (Component 3), n-heptane (Component 2), and n-octane (Component 1). Two-feed columns are common in extractive distillation applications. Furthermore, as recently discovered by Madenoor Ramapriya et al.²⁶, a large energy saving can potentially be realized when two feed streams are introduced at two different locations of the column compared to pre-mixing them to form a single feed stream.

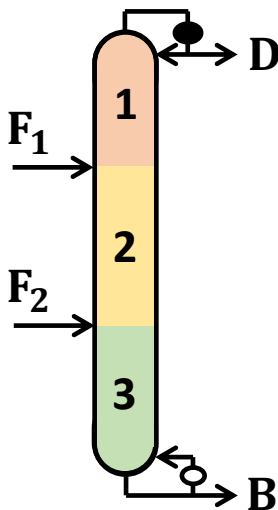


Figure 4: A two-feed column with no sidedraw product stream.

The relative volatility of each component with respect to n-octane at atmospheric pressure are estimated from Aspen Plus to be $(\alpha_3, \alpha_2, \alpha_1) = (5.1168, 2.25, 1)$. To establish a common basis for comparison, we ensure constant relative volatility and constant molar overflow assumptions by appropriately modifying the property parameters in Aspen Plus listed under PLXANT and DHVLDP²⁷. The IDEAL thermodynamic package is used. This column produces a distillate product with a total flow rate of 52.476 mol/s containing 95 mol% of n-hexane, 5 mol% of n-heptane, and negligible amount of n-octane. Thus, bottoms product has a flow rate of 147.524 mol/s containing 0.1 mol% of n-hexane, 45.671 mol% of n-heptane, and 54.229 mol% of n-octane.

We consider two scenarios in Example 1. In the first scenario, the upper feed F_1 in the MFMP column is a saturated liquid stream containing 30 mol/s of n-hexane, 60 mol/s of n-heptane, and 10 mol/s of n-octane. The lower feed F_2 is also a saturated liquid stream but with 20 mol/s of n-hexane, 10 mol/s of n-heptane, and 70 mol/s of n-octane. Clearly, F_2 is less volatile (i.e., “heavier”) than F_1 and thus has a higher bubble point temperature. Since the feed and product specifications are given, we determine that $\mathcal{I}_{F_1} = \{2, 3\}$ and $\mathcal{I}_{F_2} = \{3\}$ based on our earlier discussion in Section 2. Substituting these index sets to Algorithms 1 through 3, we obtain that the minimum reflux ratio $R_{\min} = 2.162$ and the corresponding minimum reboiler vapor duty is $V_{\text{reb}, \min} = 165.95$ mol/s. The minimum reflux condition occurs when the upper feed F_1 “controls” the separation, in which Equation (7) associated with $i = 3$ in \mathcal{I}_{F_1} becomes the binding constraint ($\gamma_3^{\text{TOP}_{F_1}} = \gamma_2^{\text{BOT}_{F_1}} = \rho_{2, F_2}$).

For this ternary separation, we can visualize its minimum reflux condition by constructing the pinch simplicies in Figure 5 based on our previous work²¹. We observe that the pinch simplicies associated with SEC_1 and SEC_2 share a common boundary, where F_1 stream composition \mathbf{x}_{F_1} also lies. This means the two boundaries of the pinch simplicies satisfy $z_3^{\text{TOP}_{F_1}}(\mathbf{x}_{F_1}) = z_2^{\text{BOT}_{F_1}}(\mathbf{x}_{F_1}) = 0$, which implies $\gamma_3^{\text{TOP}_{F_1}} = \gamma_2^{\text{BOT}_{F_1}} = \rho_{2, F_2}$ (see Figure 6 for illustration of pinch simplex; readers may refer to our previous work²¹ for detailed explanation). In other words, the geometric interpretation of feasible separation is that the pinch simplicies of any two adjacent column sections must be connected, and minimum reflux condition occurs when the pinch simplicies sandwiching the controlling feed or sidedraw stream share a common face. If the reflux ratio is further reduced, these two simplicies will no longer be connected, or $z_3^{\text{TOP}_{F_1}}(\mathbf{x}_{F_1}) < 0$, and $z_2^{\text{BOT}_{F_1}}(\mathbf{x}_{F_1}) < 0$. This indicates that $\gamma_3^{\text{TOP}_{F_1}} < \rho_{2, F_1}$ and $\gamma_2^{\text{BOT}_{F_1}} > \rho_{2, F_1}$, hence violating the feasibility constraint of Equation (7) for feed F_1 . Therefore, $R_{\min} = 2.162$ is indeed the minimum reflux ratio.

We validate the minimum reflux ratio obtained from our shortcut method using rigorous Aspen Plus simulation. Each column section contains 50 equilibrium stages, much larger than what are needed for this paraffin separation task. This is to ensure that the true minimum reflux condition is achieved. It turns out that the minimum reflux ratio obtained from our shortcut method is less than 1% different compared to true minimum reflux ratio ($R_{\min} = 2.145$) obtained from rigorous Aspen Plus simulation. Also, the liquid composition profile inside this two-feed column at minimum reflux, as shown in Figure 7, exactly follows the behavior of liquid composition trajectory bundle of a pinch simplex (see Figure 6). For more details, readers are directed to review Sections 3.4 and 4.2 of Jiang et al.²¹. Specifically, since the distillate product is free of n-octane, the liquid composition profile \mathbf{x}_n (where stage number n is numbered from top to bottom) starting from the distillate product ($n = 0$) must lie on the hyperplane $z_1^{\text{SEC}_1}(\mathbf{x}) = 0$ until it reaches a (saddle) pinch, which corresponds to vertex Z_2 of the pinch simplex and lies inside SEC_1 . Below this pinch, the liquid composition profile continues along the hyperplane $z_3^{\text{SEC}_1}(\mathbf{x}) = 0$ until it reaches the lower end of SEC_1 , which is connected to the top of SEC_2 . It turns out this is where the pinch zone lies for SEC_2 . Since the pinch is an unstable node when moving downward along the column, the liquid

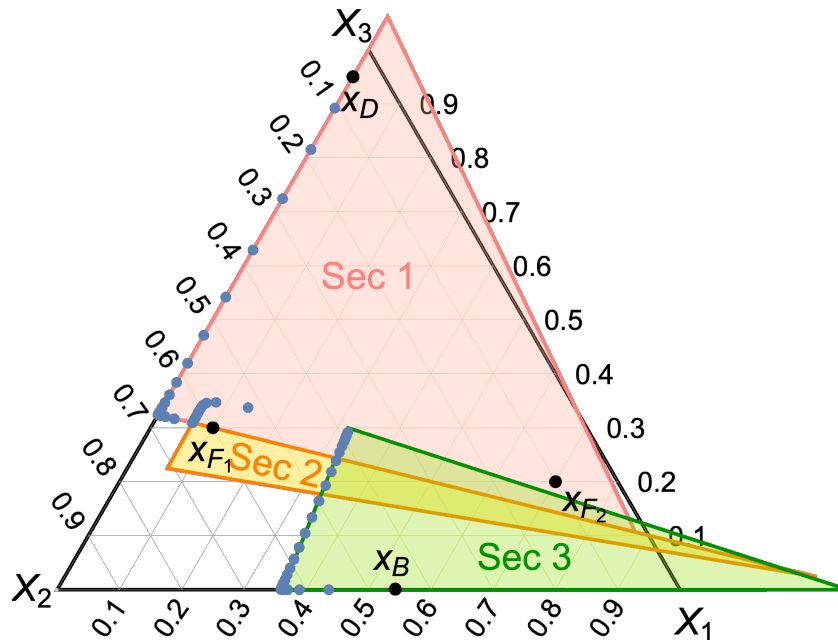


Figure 5: The pinch simplices at the minimum reflux condition obtained using Algorithms 1 through 3. Hereafter, X_1 , X_2 , X_3 represent pure n-octane, n-heptane, and n-hexane, respectively. The colors of the pinch simplices match with those in Figure 4. The blue dots are the actual liquid composition profile of this two-feed column simulated in Aspen Plus as a RadFrac column. By setting up appropriate **Design Specs** in Aspen Plus to simulate the MFMP containing 150 equilibrium stages, we obtain a minimum reflux ratio of $R_{\min} = 2.145$ from Aspen Plus. The exact pinches compositions in SEC₁ through SEC₃ are Z_2 (associated with pinch root $\gamma_p^{\text{SEC}_1} = \gamma_2^{\text{SEC}_1} \in (\alpha_1, \alpha_2)$), Z_3 (associated with pinch root $\gamma_p^{\text{SEC}_2} = \gamma_3^{\text{SEC}_2} \in (\alpha_2, \alpha_3)$), and Z_3 ($\gamma_p^{\text{SEC}_3} = \gamma_3^{\text{SEC}_3} \in (\alpha_3, \alpha_3 + \delta)$), respectively. Therefore, $\mu_2^{\text{SEC}_1} = \mu_3^{\text{SEC}_2} = \mu_4^{\text{SEC}_3} = 1$.

composition profile moves away from the pinch until it reaches the lower end of SEC₂. Again, the pinch zone of SEC₃ is located at the top of the section, from which the composition profile follows its trajectory inside the pinch simplex and heads toward the stable node (Z_1) until it reaches the bottoms product composition. It is worth noting that, while the n-hexane composition is small in the bottoms product (0.1 mol%), it is not negligible. Thus, although the liquid composition profile inside SEC₃ may appear to be approaching to the saddle point pinch, it never actually reaches the saddle pinch, which can be seen from Figure 7.

Next, using the same two-feed column example, we will examine the prevailing modeling heuristics that (1) a MFMP column can be decomposed into a series of simple columns with exactly one feed and two products, and (2) the actual minimum reflux ratio of the original MFMP column is simply the largest minimum reflux ratio value determined for all decomposed simple columns (which can be determined by applying the classic Underwood method^{28;29}). According to column decomposition, the two-feed column of Figure 4 is modeled as two simple columns, with one having F_1 as the feed stream and consisting of SEC₁ and SEC₂, whereas the other with F_2 as the feed stream and consisting of SEC₂ and SEC₃. In this case, it turns out that the largest minimum reflux ratio of the two decomposed simple columns is identified as 2.618, which is significantly higher than the true minimum reflux ratio. In other words, the column decomposition approach overestimates the true minimum reflux in this example.

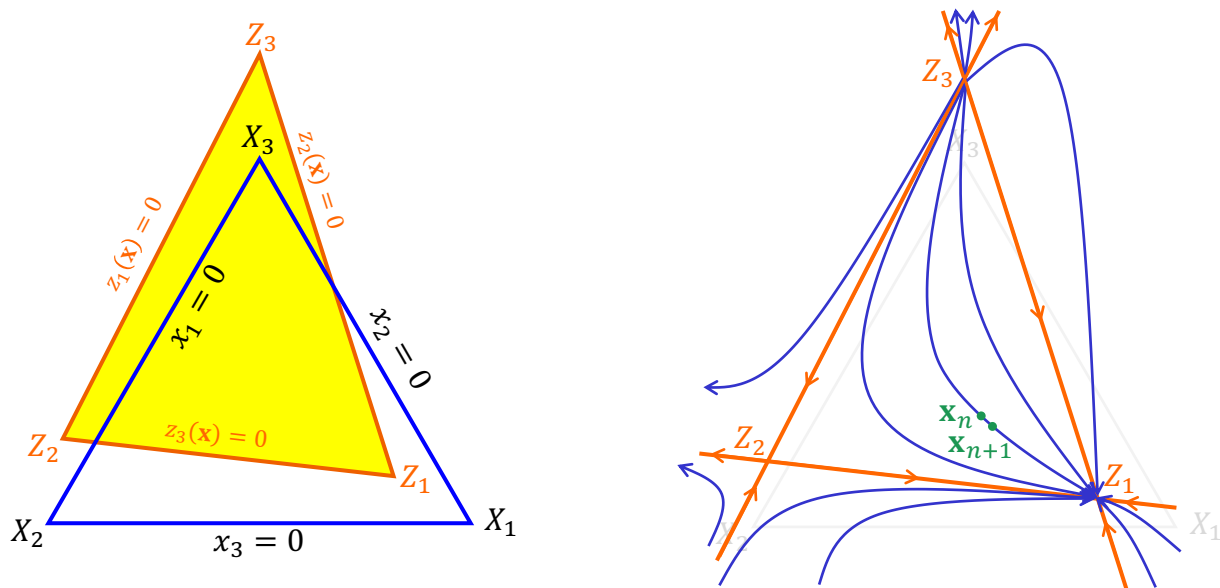


Figure 6: An illustration of pinch simplex constructed for a column section and liquid composition trajectory bundle. The pinch simplex boundary $z_i(\mathbf{x}) = 0$ is associated with the root γ_i (see Table 1 of our previous work²¹ for explanation). And possible pinch compositions are given by vertices of the pinch simplex, Z_i . The arrows indicate the direction of liquid composition evolution as we move downward from the top of the column section.

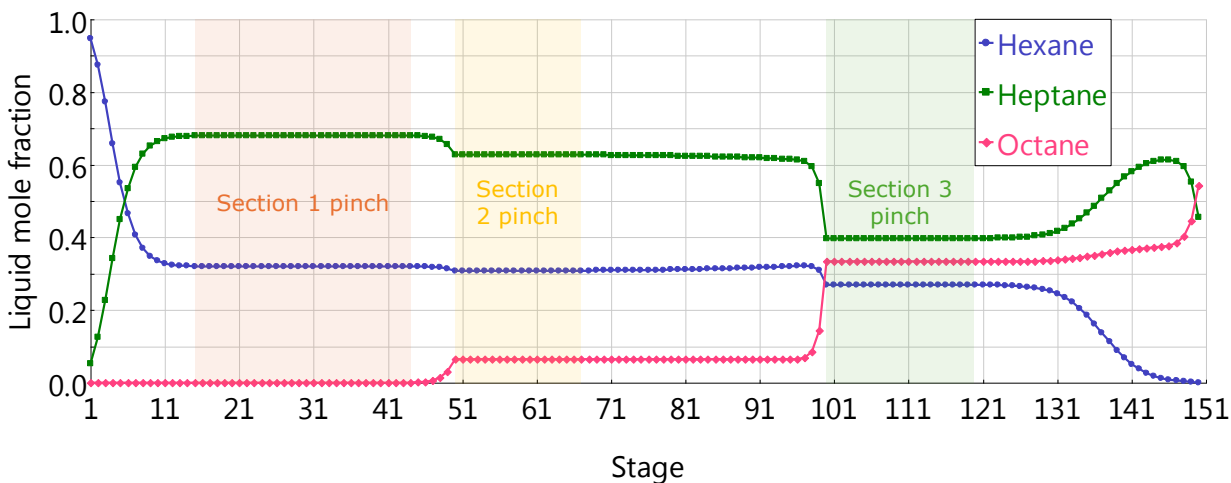


Figure 7: The liquid composition profile retrieved from Aspen Plus at the true minimum reflux ratio of $R_{\min} = 2.145$. It is clear that the pinch in SEC_1 is a saddle point and is located inside the column section, whereas the pinches in SEC_2 and SEC_3 are both unstable nodes and are located at the top of their column sections. Note that the colors of these pinch zones match with their pinch simplices drawn in Figure 5.

Now, we consider the second scenario where the locations of the two feed streams are switched. In other words, the upper feed F_1 is less volatile than the lower feed F_2 . The distillate and bottoms product specifications remain unchanged. Using Algorithms 1 through 3, we determine

that the minimum reflux ratio of this new arrangement is $R_{\min} = 1.683$, at which the lower feed F_2 controls the separation. This can be visualized from the pinch simplex diagram of Figure 8, where sections TOP_{F_2} (i.e., SEC_2) and BOT_{F_2} (i.e., SEC_3) share a common boundary, indicating that $\gamma_3^{\text{TOP}_{F_2}} = \gamma_2^{\text{BOT}_{F_2}} = \rho_{2,F_2}$ is the binding constraint. Rigorous Aspen Plus simulation shows that the true minimum reflux ratio is 1.738. Thus, our shortcut model gives an accurate estimation of the minimum reflux ratio with a 3% relative difference compared to the true minimum reflux ratio. Furthermore, if we adopt the column decomposition method, we would end up with a “minimum reflux ratio” that is as high as 19.714, which is almost 11.3 times as large as the true minimum reflux ratio! Clearly, designing or operating the MFMP column based on incorrect minimum reflux ratio will lead to tremendous capital and operating costs.

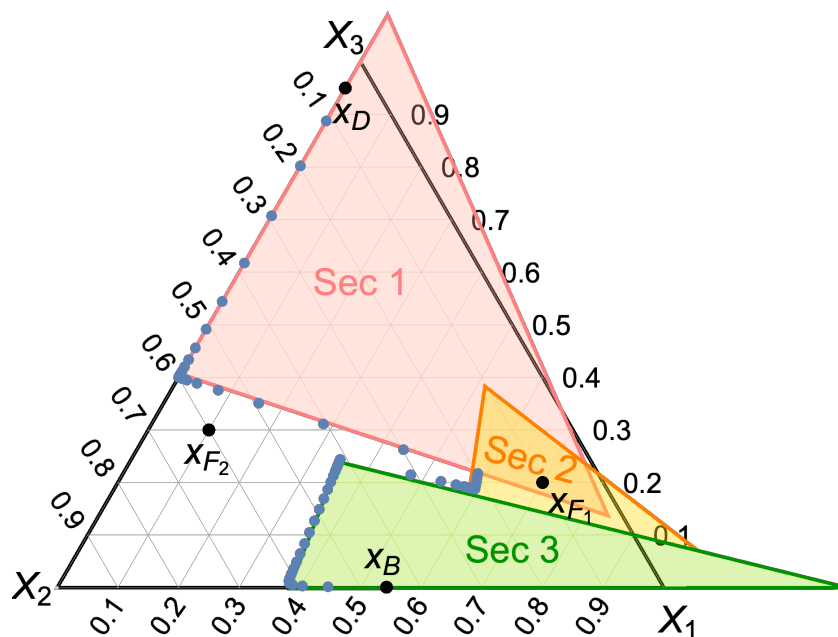


Figure 8: For the case where the upper feed is less volatile than the lower feed, the pinch simplex diagram at calculated minimum reflux ratio of $R_{\min} = 1.683$. The blue dots indicate the liquid composition profile at $R = 1.738$, which is the minimum reflux ratio predicted by rigorous Aspen Plus simulation.

By examining the two scenarios, we find that the optimal feed arrangement does not necessarily follow any particular pattern based on its temperature. Intuitively, one might think that, in order to reduce energy consumption (i.e., reflux ratio), feed streams should be placed according to their temperatures. Specifically, a common belief is that a high-temperature feed should be placed closer to the bottom of the column than a low-temperature feed. However, it turns out that, despite achieving the same product flow rates and purities, the minimum reflux ratio in the first scenario ($R_{\min} = 2.162$) is much higher than that in the second scenario ($R_{\min} = 1.683$)! This finding matches with the observation first made by Levy and Doherty³⁰. And here we provide the first systematic analysis of the contradictions to the common belief that a high-temperature feed should be placed below a low-temperature feed. Practitioners should examine carefully the optimal feed arrangement when designing their columns. In this regard, our shortcut model and minimum reflux calculation method allow practitioners to obtain a quick and reliable screening of the optimal feed arrangement.

5.2 Example 2: A One-Feed, Two-(Side)Product Column

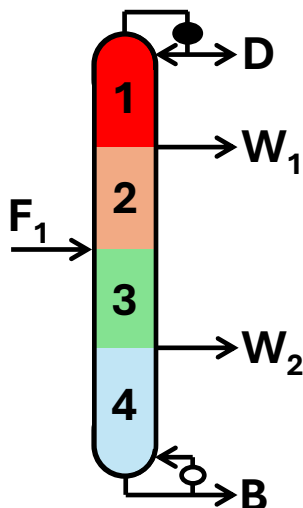


Figure 9: A one-feed column with two sidedraw streams considered in Example 2. The colors of the pinch simplices match with those in Figure 9.

In this example, we study a distillation column separating a ternary mixture of n-hexane, n-heptane, and n-octane with one feed stream and two sidedraw product streams, as shown in Figure 9. When there is only one feed stream and both sidedraw products are withdrawn as saturated liquids, there is a common belief in the literature (e.g., Sugie and Lu³¹, Glinos and Malone³²) that F_1 will always be “controlling” the separation at minimum reflux. This assumption originates from the observation of the McCabe-Thiele diagram for binary distillation with saturated liquid sidedraws, where the operating lines for sections above F_1 continuously decreases from the top of the column to F_1 , and the operating lines for sections below F_1 continuously increases from the bottom of the column to F_1 .

To verify if this result can be generalized to multicomponent distillation, we present this example where F_1 is a saturated liquid stream containing 30 mol/s of n-hexane (Component 3), 40 mol/s of n-heptane (Component 2), and 30 mol/s of n-octane (Component 1). The distillate stream contains 24 mol/s of n-hexane, 6 mol/s of n-heptane and negligible amount of n-octane, whereas the bottoms product contains 20 mol/s of n-octane and no n-hexane or n-heptane. The upper sidedraw W_1 , which is located above F_1 , is a saturated liquid stream with 6 mol/s of n-hexane and 24 mol/s of n-heptane. The lower sidedraw W_2 is also a saturated liquid stream with 10 mol/s of n-heptane and 10 mol/s of n-octane. Once $\{d_i^{\text{SEC}_k}\}_{i,k}$ are determined, we determine that $\mathcal{I}_{W_1} = \{2\}$, $\mathcal{I}_{F_1} = \{2, 3\}$, $\mathcal{I}_{W_2} = \{2, 3\}$.

By applying Algorithms 1 through 3, we determine that the minimum reflux ratio is $R_{\min} = 2.693$, which is less than 1% different compared to rigorous Aspen Plus simulation minimum reflux ratio result of 2.668. From the minimum reflux pinch simplex diagram of Figure 10, we can see that sidedraw W_1 actually controls the separation at minimum reflux. Specifically, the minimum reflux occurs when $z_2^{\text{TOP}_{W_1}}(\mathbf{x}_{W_1}) = z_2^{\text{BOT}_{W_1}}(\mathbf{x}_{W_1}) = 0$, indicating that $\gamma_3^{\text{TOP}_{W_1}} = \gamma_3^{\text{BOT}_{W_1}} = \rho_{2,W_1}$. This is a consequence of Equation (15), which requires that the sidedraw composition \mathbf{x}_{W_1} must lie on the liquid composition profile, and thus must not reside outside of the pinch simplices associated with SEC_1 and SEC_2 . If the reflux ratio drops below this minimum threshold, the sidedraw composition \mathbf{x}_{W_1} no longer resides within the pinch simplices, as their boundaries

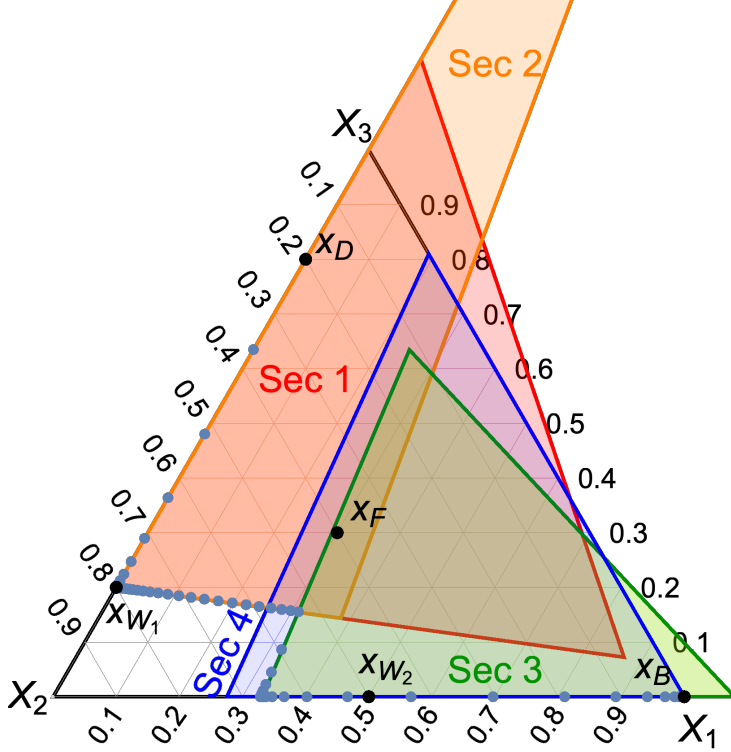


Figure 10: The pinch simplex diagram for a one-feed, two-(side)product column example at minimum reflux ($R_{\min} = 2.693$), along with the liquid composition profile at the minimum reflux of $R_{\min} = 2.668$ identified by Aspen Plus (also see Figure 11). The exact pinches compositions in SEC₁ through SEC₄ are Z_2 (associated with pinch root $\gamma_p^{\text{SEC}_1} = \gamma_2^{\text{SEC}_1} \in (\alpha_1, \alpha_2)$), Z_2 (associated with pinch root $\gamma_p^{\text{SEC}_2} = \gamma_2^{\text{SEC}_2} \in (\alpha_1, \alpha_2)$), Z_2 (associated with pinch root $\gamma_p^{\text{SEC}_3} = \gamma_2^{\text{SEC}_3} \in (\alpha_2, \alpha_3)$), and Z_1 ($\gamma_p^{\text{SEC}_4} = \gamma_1^{\text{SEC}_4} \in (\alpha_1, \alpha_2)$), respectively. Therefore, $\mu_2^{\text{SEC}_1} = \mu_2^{\text{SEC}_2} = \mu_3^{\text{SEC}_3} = \mu_2^{\text{SEC}_4} = 1$.

$z_3^{\text{TOP}_{w_1}}(\mathbf{x}) = 0$ and $z_3^{\text{BOT}_{w_1}}(\mathbf{x}) = 0$ would move toward X_3 (pure n-hexane).

Now, to see what happens when we insist F_1 to control the separation at minimum reflux, we relax the feasibility constraints in Algorithms 1 through 3 by ignoring Equation (15). This gives a “minimum reflux ratio” of 2.533, which is lower than the true minimum reflux ratio. As a result, we have provided a counterexample to the common belief that the feed stream always controls the minimum reflux operation when sidedraws are taken as saturated liquid streams. Without incorporating the constraints related to sidedraws, one may completely ignore the possibility that a sidedraw could control the separation at minimum reflux and thus will obtain an incorrect minimum reflux ratio value that causes infeasible separation. To the best of our knowledge, this work is the first in deriving these sidedraw-related constraints and incorporating them in an algorithmic framework to calculate the true minimum reflux ratio for MFMP columns. Furthermore, we remark that our proposed minimum reflux calculation method is a generalized framework that is not limited to single-feed columns in saturated liquid sidedraws.

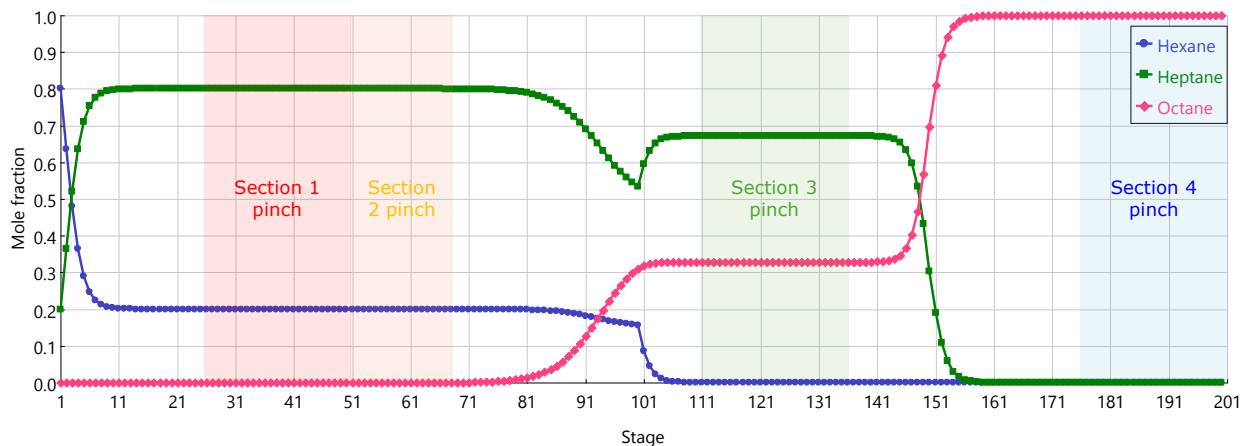


Figure 11: The liquid composition profile retrieved from Aspen Plus at the true minimum reflux ratio $R_{\min} = 2.668$. Each of the four column sections are given 50 equilibrium stages. The pinch zones in SEC_1 through SEC_4 are located respectively at the bottom, at the top, within, and at the bottom of their corresponding column sections. Note that the colors of these pinch zones match with their pinch simplices drawn in Figure 10.

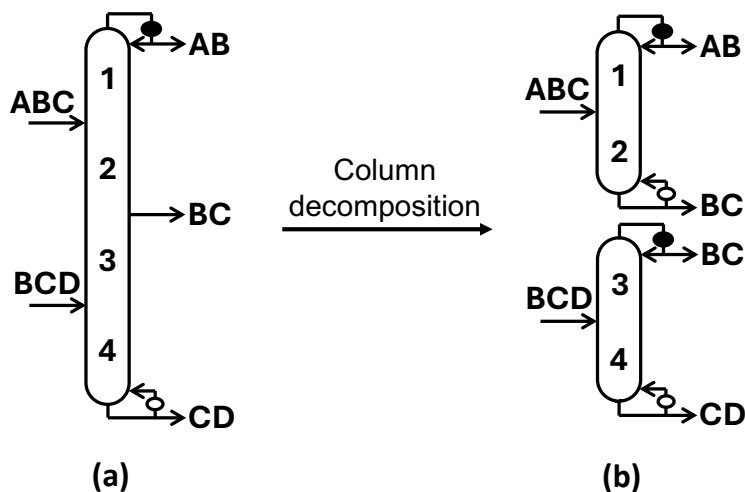


Figure 12: (a) A MFMP column for quaternary separation; (b) the decomposed version of (a).

5.3 Example 3: A Two-Feed, One-(Side)Product Column

In the third example, we study a MFMP column drawn in Figure 12a that separates n-hexane (component A or 4), n-heptane (component B or 3), n-octane (component C or 2), and n-nonane (component D or 1). The relative volatilities with respect to nonane is are $(\alpha_4, \alpha_3, \alpha_2, \alpha_1) = (12.332, 5.361, 2.300, 1)$. Such a MFMP column are very common in multicomponent distillation configurations⁴, and it can be obtained by consolidating two simple columns and merging the common product stream BC into a sidestream. For this MFMP column, the upper feed F_1 (ABC) is a saturated vapor stream with 30 mol/s of n-hexane (component A), 30 mol/s of n-heptane (component B), and 40 mol/s of n-octane (component C), whereas the lower feed F_2 (BCD) is a saturated liquid stream with 40 mol/s of n-heptane, 30 mol/s of n-octane, and 30 mol/s of n-nonane (component D). The sidestream W_1 (BC) is in saturated liquid state. In terms of

product specifications, we require that the most volatile component A must be completely recovered in the distillate stream, whereas the least volatile component D must be completely recovered in the bottoms product. The distributions of intermediate components B and C in product streams, on the other hand, are flexible. Depending on what the distributions are, component B in SEC₂ and component C in SEC₃ could have either net material upward or downward flow. For instance, when component B in SEC₂ has net material upward flow ($d_3^{\text{SEC}_2} > 0$), some of component B coming from the lower feed F₂ will travel all the way to the top of the column and be produced as distillate. Because of this, the pinch root $\gamma_p^{\text{SEC}_2} = \gamma_3^{\text{SEC}_2}$ may lie in either (α_2, α_3) or (α_3, α_4) . Similarly, the pinch root $\gamma_p^{\text{SEC}_3} = \gamma_2^{\text{SEC}_3}$ may lie in either (α_1, α_2) or (α_2, α_3) . As a result, we only need one binary variable, $\mu_3^{\text{SEC}_2}$, to indicate whether $\gamma_p^{\text{SEC}_2}$ lies in (α_2, α_3) or not. Similarly, we also only need one binary variable, $\mu_2^{\text{SEC}_3}$, to indicate whether $\gamma_p^{\text{SEC}_3}$ lies in (α_1, α_2) or not.

Furthermore, since $\gamma_3^{\text{SEC}_2} \in (\alpha_2, \alpha_4)$ and $\gamma_2^{\text{SEC}_3} \in (\alpha_1, \alpha_3)$, singularity issue might arise when implementing Equation (1) in the optimization model when pinch root $\gamma_3^{\text{SEC}_2}$ takes the value α_3 and/or when pinch root $\gamma_2^{\text{SEC}_3}$ takes the value α_2 . To avoid the singularity issue, we reformulate Equation (1) by multiplying both sides of it by the bound factor (e.g., $(\alpha_3 - \gamma_3^{\text{SEC}_2})$ for V^{SEC_2}) followed by performing partial fraction decomposition. For example, the V^{SEC_2} expression can be reformulated as:

$$\begin{aligned} V^{\text{SEC}_2}(\alpha_3 - \gamma_3^{\text{SEC}_2}) &= (\alpha_3 - \gamma_3^{\text{SEC}_2}) \frac{\alpha_2 d_2^{\text{SEC}_2}}{\alpha_2 - \gamma_3^{\text{SEC}_2}} + \alpha_3 d_3^{\text{SEC}_2} \\ &= \alpha_2 d_2^{\text{SEC}_2} + (\alpha_3 - \alpha_2) \frac{\alpha_2 d_2^{\text{SEC}_2}}{\alpha_2 - \gamma_3^{\text{SEC}_2}} + \alpha_3 d_3^{\text{SEC}_2}, \end{aligned}$$

which we note that $d_1^{\text{SEC}_2} = d_4^{\text{SEC}_2} = 0$ because n-hexane is completely recovered in the distillate stream and n-nonane is completely recovered in the bottoms stream, as shown in Figure 12. Similarly, we can reformulate the V^{SEC_3} expression using this technique. With this, we can safely bound $\gamma_3^{\text{SEC}_2} \in (\alpha_2, \alpha_4)$ and $\gamma_2^{\text{SEC}_3} \in (\alpha_1, \alpha_3)$ without concerning about the singularity issue. In Appendix C, we provide all the equations and constraints needed to determine the optimal distribution of intermediate components to minimize the reboiler vapor duty requirement (i.e., V^{SEC_4}) for this MFMP column. The resulting optimization model, which is a mixed-integer nonlinear program (MINLP), is solved to global optimality within 15 CPU seconds in a Dell Precision 7865 workstation (equipped with 128 GB RAM and AMD Ryzen Threadripper PRO 5975WX 32-Cores 3.6 GHz processor) using global solver BARON 24.3²⁵ via GAMS 46.5. In Appendix C, we provide the complete MINLP formulation implemented in GAMS. The lowest possible minimum reboiler vapor duty $V_{\text{reb},\text{min}}$ (i.e., minimum vapor duty in SEC₄) is determined to be 71.87 mol/s. And the corresponding optimal product distributions are summarized in Table 1.

Stream	Label in Figure 12a	Flow rate of component A, B, C, D (mol/s)
Distillate	AB	30, 14.23, 0, 0
Sidedraw	BC	0, 55.77, 48.94, 0
Bottoms	CD	0, 0, 21.06, 30

Table 1: Optimal distributions of n-hexane, n-heptane, n-octane, and n-nonane in all product streams at $V_{\text{reb},\text{min}} = 71.87$ mol/s. One can determine that $d_4^{\text{SEC}_2} = 0$ and $d_3^{\text{SEC}_2} = -15.77$ mol/s < 0, and thus $\mu_4^{\text{SEC}_2} = 1$. Meanwhile, $d_2^{\text{SEC}_3} = 8.94$ mol/s > 0 and $d_1^{\text{SEC}_3} = 0$, and thus $\mu_2^{\text{SEC}_3} = 1$.

We verify this result by performing exhaustive sensitivity analysis using Aspen Plus. The lowest reboiler vapor duty requirement that satisfies product requirements is found to be 77.9 mol/s, which is within 8.3% relative difference compared to the MINLP result. The associated n-heptane and n-octane flow rates in product streams also match very well with the results shown in Table 1. This validates the accuracy and computationally efficiency of global optimization framework based on the shortcut model. Moreover, we remark that the global optimization algorithm does more than just finding the minimum energy requirement of a MFMP column and its corresponding product distributions. For example, there has been a lingering question among the distillation community of whether all n-heptane can be recovered from the distillate product in this MFMP column. We can easily answer questions like this by modifying the relevant variable bounds and/or by adding/deactivating related constraints in the MINLP formulation. In this case, by introducing a new constraint $d_3^{\text{SEC}1} = f_{3,F_1} + f_{3,F_2}$ into the MINLP formulation, the resulting optimization problem turns out to be infeasible. Thus, we conclude that it is impossible to recover all the n-heptane in the distillate product. Rigorous Aspen Plus simulation also confirms that some n-heptane is always drawn from the sidedraw no matter how much vapor is generated at the reboiler.

Stream	Label in Figure 12a	Flow rate of component A, B, C, D (mol/s)
Distillate	AB	30, 40, 0, 0
Sidedraw	BC	0, 30, 40, 0
Bottoms	CD	0, 0, 30, 30

Table 2: Component molar flow rates (arranged as n-hexane, n-heptane, n-octane, and lastly n-nonane) of all product streams.

Lastly, using this MFMP column as an example, we illustrate why the column decomposition method shown in Figure 12 fails to calculate the true minimum reflux ratio. The product flow rates and compositions in this example have already been specified and are listed in Table 2. The minimum reflux ratio (which is also achieved when reboiler vapor duty is minimized as product flow rates are fixed) can be calculated using Algorithm 1 or approach. In particular, it is worth mentioning that the resulting optimization program is solved to global optimality instantaneously during preprocessing step. Both approaches give the same minimum reflux ratio of $R_{\min} = 2.002$, which is only 0.1% different from the minimum reflux ratio of 2.000 predicted by Aspen Plus simulation. Furthermore, this is achieved when sidedraw BC controls the minimum reflux condition. Meanwhile, the column decomposition method, which calculates the minimum reflux ratio of two simple columns as shown in Figure 12b using the classic Underwood method, yields a “minimum reflux ratio” of 1.806, which is significantly lower than the true minimum reflux ratio. In other words, if the column operates at $R = 1.806$, the desired separation can never be achieved.

There are two main reasons why column decomposition technique fails in this example. First, from Table 2, one can calculate that the component distillate flow for n-heptane (B) is greater than n-heptane flow rate in the upper feed F_1 . This means that some of n-heptane in the distillate must come from the lower feed F_2 . Likewise, since the component bottoms flow for n-octane (C) is greater than the n-octane flow rate in the lower feed, some of n-octane in the bottoms must come from the upper feed F_1 . Therefore, in this MFMP column, components with intermediate relative volatilities do not follow the same flow pattern when the MFMP column is decomposed into two single columns. The second reason is that, as the original MFMP column is decomposed into two simple columns, we lose the possibility that stream BC may control the minimum reflux. Therefore, we must consider the entire MFMP column as a whole when modeling its separation performance

and determining its minimum reflux condition, using methods such as the one presented in this work.

6 Conclusion

In this paper, we introduce the mathematical formulation that incorporates the model developed in the first article of the series²¹ to determine the minimum reflux condition of MFMP columns for multicomponent distillation. When the full product specifications are given, an algorithmic procedure is developed to automatically determine the minimum reflux ratio or minimum reboiler vapor duty requirement. When some of the product specifications are not given to users a priori, an optimization model can be developed as an MINLP to simultaneously identify the minimum reflux ratio and the corresponding optimal product distributions. We present the use of both approaches to analyze the minimum reflux behavior of MFMP columns. In all case studies, our minimum reflux ratio results matches very well with rigorous Aspen Plus simulation results.

In addition to validating the accuracy and usefulness of our proposed algorithmic and optimization frameworks, the second aim of these case studies is to reexamine some of the well-accepted design heuristics and modeling assumptions the distillation community has been relying on regarding how MFMP columns should be designed and operated. It turns out that some of these heuristics and assumptions need to be rewritten. In Example 1, we show a counterexample where placing a colder feed stream above a warmer feed stream, which follows the temperature profile within the column, actually leads to a higher minimum vapor duty requirement than if the feed stream locations are reversed. Thus, we must analyze all possible permutations of relative feed locations to determine the optimal feed stream arrangement. Our shortcut based approach is particularly suitable for analyses like this compared to rigorous process simulations which can be quite time consuming to perform, especially as the number of feed streams and/or sidedraw streams increases.

Another key finding is that decomposing a MFMP column into multiple simple columns and taking the largest individual minimum reflux ratios of each decomposed column using the classic Underwood method is not the correct approach to determine the minimum reflux ratio of the original MFMP column. In fact, such column decomposition approach can lead to minimum reflux ratio values that significantly deviate from the true minimum reflux ratio. On the other hand, our shortcut based approach considers the entire MFMP column as a whole, which is needed for accurately estimating the true minimum reflux ratio.

Finally, when a distillation column has one or more sidedraw streams, one of the sidedraw streams can control the separation at minimum reflux, even when they are all withdrawn as saturated liquid streams. This possibility has often been overlooked by the distillation community in the past due to the lack of fundamental understanding and systematic tools to model how sidedraws affect the minimum reflux operation of a multicomponent distillation column. The mathematical model and algorithms developed in this series have filled this gap, thus allowing practitioners to conduct rigorous, accurate analysis of columns with sidedraws for the first time. Overall, we believe that these new findings and insights are helpful in synthesizing and operating energy-efficient, cost-competitive, and intensified MFMP columns for multicomponent distillation.

Acknowledgment

The information, data, or work presented herein was funded in part by the start-up fund from College of Engineering, Architecture, and Technology at Oklahoma State University.

Data Availability and Reproducibility Statement

The liquid composition data obtained from rigorous Aspen Plus simulations are transformed into the equilateral triangular coordinate as shown in Figures 5, 8, and 10 to be visualized. The transformed liquid composition data are provided in the Supplementary Material. The procedure and specifications used to produce the pinch simplices for all column sections are provided in Algorithms 1 through 3 within the article. The optimal product distribution results in Table 1 are obtained by the MINLP formulation provided in Appendix C.

References

- 1 Górak A, Olujić Z. Distillation: Fundamentals and Principles. Elsevier Inc. 2014.
- 2 US DOE Industrial Efficiency & Decarbonization Office. Manufacturing Energy and Carbon Footprints (2018 MECS). 2021.
- 3 US DOE. Industrial Decarbonization Roadmap. 2022.
- 4 Shah VH, Agrawal R. A matrix method for multicomponent distillation sequences. AICHE Journal. 2010;56(7):1759–1775.
- 5 Nallasivam U, Shah VH, Shenvi AA, Tawarmalani M, Agrawal R. Global optimization of multicomponent distillation configurations: 1. Need for a reliable global optimization algorithm. AICHE Journal. 2013;59(3):971–981.
- 6 Nallasivam U, Shah VH, Shenvi AA, Huff J, Tawarmalani M, Agrawal R. Global optimization of multicomponent distillation configurations: 2. Enumeration based global minimization algorithm. AICHE Journal. 2016;62(6):2071–2086.
- 7 Jiang Z, Agrawal R. Process intensification in multicomponent distillation: A review of recent advancements. Chemical Engineering Research and Design. 2019;147:122–145.
- 8 Jiang G Zheyuand Madenoor Ramapriya, Tawarmalani M, Agrawal R. Process intensification in multicomponent distillation. Chemical Engineering Transactions. 2018;69:841–846.
- 9 Agrawal R, Tumbalam Gooty R. Misconceptions about efficiency and maturity of distillation. AICHE Journal. 2020;66(8):e16294.
- 10 Agrawal R, Yee TF. Heat Pumps for Thermally Linked Distillation Columns: An Exercise for Argon Production from Air. Industrial & Engineering Chemistry Research. 1994;33(11):2717–2730.
- 11 Nogaja A, Tawarmalani M, Agrawal R. Distillation Electrification Through Optimal Use of Heat Pumps. In: 34th European Symposium on Computer Aided Process Engineering / 15th

- International Symposium on Process Systems Engineering, edited by Manenti F, Reklaitis GV, vol. 53 of Computer Aided Chemical Engineering, pp. 1297–1302. Elsevier. 2024;.
- 12 Wankat PC. Multieffect distillation processes. Industrial & Engineering Chemistry Research. 1993;32(5):894–905.
 - 13 Agrawal R, Herron DM. Intermediate reboiler and condenser arrangement for binary distillation columns. AIChE Journal. 1998;44(6):1316–1324.
 - 14 Agrawal R, Fidkowski ZT, Xu J. Prefractionation to reduce energy consumption in distillation without changing utility temperatures. AIChE Journal. 1996;42(8):2118–2127.
 - 15 Agrawal R, Herron DM. Optimal thermodynamic feed conditions for distillation of ideal binary mixtures. AIChE Journal. 1997;43(11):2984–2996.
 - 16 Jiang Z, Madenoor Ramapriya G, Tawarmalani M, Agrawal R. Minimum energy of multicomponent distillation systems using minimum additional heat and mass integration sections. AIChE Journal. 2018;64(9):3410–3418.
 - 17 Tumbalam Gooty R, Chavez Velasco JA, Agrawal R. Methods to assess numerous distillation schemes for binary mixtures. Chemical Engineering Research and Design. 2021;172:1–20.
 - 18 Chavez Velasco JA, Tawarmalani M, Agrawal R. Systematic Analysis Reveals Thermal Separations Are Not Necessarily Most Energy Intensive. Joule. 2021;5(2):330–343.
 - 19 Gilliland ER. MULTICOMPONENT RECTIFICATION. Industrial & Engineering Chemistry. 1940;32(8):1101–1106.
 - 20 Doherty MF. Conceptual design of distillation systems. McGraw-Hill chemical engineering series. Boston: McGraw-Hill. 2001.
 - 21 Jiang Z, Tawarmalani M, Agrawal R. Minimum reflux calculation for multicomponent distillation in multi-feed, multi-product columns: Mathematical model. AIChE Journal. 2022; 68(12):e17929.
 - 22 Mathew TJ, Tawarmalani M, Agrawal R. Relaxing the constant molar overflow assumption in distillation optimization. AIChE Journal. 2023;69(9):e18125.
 - 23 Jiang Z, Mathew TJ, Zhang H, Huff J, Nallasivam U, Tawarmalani M, Agrawal R. Global optimization of multicomponent distillation configurations: Global minimization of total cost for multicomponent mixture separations. Computers & Chemical Engineering. 2019;126:249–262.
 - 24 Jiang Z, Chen Z, Huff J, Shenvi AA, Tawarmalani M, Agrawal R. Global minimization of total exergy loss of multicomponent distillation configurations. AIChE Journal. 2019;65(11):e16737.
 - 25 Tawarmalani M, Sahinidis NV. A polyhedral branch-and-cut approach to global optimization. Mathematical Programming. 2005;103:225–249.
 - 26 Madenoor RG, Mohit T, Rakesh A. Modified basic distillation configurations with intermediate sections for energy savings. AIChE Journal. 2014;60(3):1091–1097.
 - 27 Shah VH. Energy savings in distillation via identification of useful configurations. Ph.D. thesis, Purdue University. 2010.

- 28 Underwood AJV. Fractional Distillation of Multicomponent Mixtures. Industrial & Engineering Chemistry. 1949;41(12):2844–2847.
- 29 Underwood AJV. Fractional distillation of multicomponent mixtures. Chemical Engineering Progress. 1948;44:603–614.
- 30 Levy SG, Doherty MF. Design and synthesis of homogeneous azeotropic distillations. 4. Minimum reflux calculations for multiple-feed columns. Industrial & Engineering Chemistry Fundamentals. 1986;25(2):269–279.
- 31 Sugie H, Lu B. On the determination of minimum reflux ratio for a multicomponent distillation column with any number of side-cut streams. Chemical Engineering Science. 1970;25(12):1837–1846.
- 32 Glinos KN, Malone MF. Design of sidestream distillation columns. Industrial & Engineering Chemistry Process Design and Development. 1985;24(3):822–828.

A Parameters and Variables

c	Total number of components present in the distillation column
α_i	Relative volatility of component i with respect to the heaviest component
$d_i^{\text{SEC}_k}$	Component i 's net material upward flow in column section k
V^{SEC_k}	Total vapor flow in column section k
$\gamma_i^{\text{SEC}_k}$	The i^{th} root of Equation (1)
p^{SEC_k}	The pinch index of section k
$\gamma_p^{\text{SEC}_k}$	The pinch root of section k
\mathbf{x}_n	The vector of liquid composition leaving stage n
X_i	The composition of pure component i
\mathbf{x}_{F_j}	Liquid composition (or hypothetical liquid composition) composition of j^{th} feed stream
\mathbf{x}_{W_j}	Liquid composition (or hypothetical liquid composition) of j^{th} sidedraw stream
$\rho_{i,F_j}, \rho_{i,W_j}$	The i^{th} root defined in Equations (8) and (13), respectively
V_{F_j}, V_{W_j}	Total vapor flow rate in the j^{th} feed and sidedraw stream, respectively
f_{i,F_j}, f_{i,W_j}	Component i 's flow rate in the j^{th} feed and sidedraw stream, respectively
l_{m,F_j}, l_{m,W_j}	Component m 's flow rate in the liquid portion of the j^{th} feed and sidedraw, respectively
v_{m,F_j}, v_{m,W_j}	Component m 's flow rate in the vapor portion of the j^{th} feed and sidedraw, respectively
N_F	Number of feed streams in the column
N_W	Number of sidedraw streams in the column
N_{SEC}	Number of column sections in the column, which is equal to $N_F + N_W + 1$
$\mu_i^{\text{SEC}_k}$	Binary variable that equals 1 when $\gamma_p^{\text{SEC}_k} \in (\alpha_{i-1}, \alpha_i)$, and 0 otherwise
$K_i^{\text{SEC}_k}$	Binary variable defined in Equation (5) and used in Equations (9), (14) and (15)

B Sets and Notations

\mathcal{C}	$\{1, \dots, c\}$
F_j, W_j	The j^{th} feed and sidedraw stream (both counting from the top), respectively
\mathcal{I}_{F_j}	Index set defined in Equation (6) for feasibility constraints associated with the j^{th} feed stream
\mathcal{I}_{W_j}	Index set defined in Equation (11) for feasibility constraints associated with the j^{th} sidedraw
TOP_{F_j}	Column section above the j^{th} feed stream
BOT_{F_j}	Column section below the j^{th} feed stream
TOP_{W_j}	Column section above the j^{th} sidedraw stream, respectively
BOT_{W_j}	Column section below the j^{th} sidedraw stream, respectively

C Optimization Model

Here, we provide the complete formulation for identifying the minimum reboiler vapor duty and the corresponding product distributions for the column shown in Figure 4.

Objective function:

$$\text{minimize } V^{\text{SEC}_4}$$

Constraints and bounds:

1. Mass balance equations and feed and product specifications:

$$\begin{aligned} f_{i,F_1} + f_{i,F_2} &= d_i^{\text{SEC}_1} - f_{i,W_1} - d_i^{\text{SEC}_4} & \forall i = 1, \dots, 4 \\ d_i^{\text{SEC}_2} &= d_i^{\text{SEC}_1} - f_{i,F_1}; \quad d_i^{\text{SEC}_3} = d_i^{\text{SEC}_2} - f_{i,W_1}; \quad d_i^{\text{SEC}_4} = d_i^{\text{SEC}_3} - f_{i,F_2} & \forall i = 1, \dots, 4 \\ f_{4,F_1} &= d_4^{\text{SEC}_1} = 30; \quad f_{1,F_2} = -d_1^{\text{SEC}_4} = 30 \\ d_1^{\text{SEC}_1} &= d_2^{\text{SEC}_1} = 0; \quad d_1^{\text{SEC}_2} = d_4^{\text{SEC}_2} = 0; \quad d_1^{\text{SEC}_3} = d_4^{\text{SEC}_3} = 0; \quad d_4^{\text{SEC}_4} = d_3^{\text{SEC}_4} = 0; \\ f_{3,F_1} &= 30; \quad f_{2,F_1} = 40; \quad f_{1,F_1} = 0; \quad f_{4,F_2} = 0; \quad f_{3,F_2} = 40; \quad f_{2,F_2} = 30; \\ d_i^{\text{SEC}_1} &\geq 0; \quad f_{i,W_1} \leq 0; \quad d_i^{\text{SEC}_4} \leq 0 & \forall i = 1, \dots, 4 \end{aligned}$$

2. Vapor duty calculations based on Equation (1):

$$\begin{aligned}
V^{\text{SEC}_1} &= \sum_{i=1}^4 \frac{\alpha_i d_i^{\text{SEC}_1}}{\alpha_i - \gamma_4^{\text{SEC}_1}} \\
V^{\text{SEC}_1} &= \sum_{i=1}^4 \frac{\alpha_i d_i^{\text{SEC}_1}}{\alpha_i - \gamma_3^{\text{SEC}_1}} \\
V^{\text{SEC}_2}(\alpha_3 - \gamma_3^{\text{SEC}_2}) &= \alpha_2 d_2^{\text{SEC}_2} + (\alpha_3 - \alpha_2) \frac{\alpha_2 d_2^{\text{SEC}_2}}{\alpha_2 - \gamma_3^{\text{SEC}_2}} + \alpha_3 d_3^{\text{SEC}_2} \\
V^{\text{SEC}_2} &= \sum_{i=1}^4 \frac{\alpha_i d_i^{\text{SEC}_2}}{\alpha_i - \gamma_2^{\text{SEC}_2}} \\
V^{\text{SEC}_3}(\alpha_2 - \gamma_2^{\text{SEC}_3}) &= \alpha_2 d_2^{\text{SEC}_3} - (\alpha_3 - \alpha_2) \frac{\alpha_3 d_3^{\text{SEC}_3}}{\alpha_3 - \gamma_2^{\text{SEC}_3}} + \alpha_3 d_3^{\text{SEC}_3} \\
V^{\text{SEC}_3} &= \sum_{i=1}^4 \frac{\alpha_i d_i^{\text{SEC}_3}}{\alpha_i - \gamma_3^{\text{SEC}_3}} \\
V^{\text{SEC}_4} &= \sum_{i=1}^4 \frac{\alpha_i d_i^{\text{SEC}_4}}{\alpha_i - \gamma_1^{\text{SEC}_4}} \\
V^{\text{SEC}_4} &= \sum_{i=1}^4 \frac{\alpha_i d_i^{\text{SEC}_4}}{\alpha_i - \gamma_2^{\text{SEC}_4}}
\end{aligned}$$

Note that here, only a subset of $\gamma_i^{\text{SEC}_k}$ roots for each section need to be defined as decision variables, as others are fixed to the respective relative volatility values due to Equation (2). For example, $\gamma_2^{\text{SEC}_1} = \alpha_2$ and $\gamma_1^{\text{SEC}_1} = \alpha_1$, since the distillate product contains no n-octane and nonane components ($d_2^{\text{SEC}_1} = d_1^{\text{SEC}_1} = 0$).

3. Defining equations for the feed and sidedraw streams:

$$\begin{aligned}
V_{F_1} = 100 &= \sum_{i=1}^4 \frac{\alpha_i f_{i,F_1}}{\alpha_i - \rho_{j,F_1}} \quad \forall j = 2, 3 \\
V_{F_2} = 0 &= \sum_{i=1}^4 \frac{\alpha_i f_{i,F_2}}{\alpha_i - \rho_{j,F_2}} \quad \forall j = 1, 2 \\
V_{W_1} = 0 &= \sum_{i=1}^4 \frac{\alpha_i f_{i,W_1}}{\alpha_i - \rho_{j,W_1}} \quad \forall j = 2
\end{aligned}$$

4. Variable bounds:

$$\begin{aligned}
\gamma_3^{\text{SEC}_1} &\in (\alpha_2, \alpha_3); \gamma_4^{\text{SEC}_1} \in (\alpha_3, \alpha_4) \\
\gamma_2^{\text{SEC}_2} &\in (\alpha_2, \alpha_3); \gamma_3^{\text{SEC}_2} \in (\alpha_2, \alpha_4) \\
\gamma_2^{\text{SEC}_3} &\in (\alpha_1, \alpha_3); \gamma_3^{\text{SEC}_3} \in (\alpha_2, \alpha_3) \\
\gamma_1^{\text{SEC}_4} &\in (\alpha_1, \alpha_2); \gamma_2^{\text{SEC}_4} \in (\alpha_2, \alpha_3) \\
\rho_{1,\text{F}_2} &\in (\alpha_1, \alpha_2); \rho_{2,\text{F}_1}, \rho_{2,\text{W}_1}, \rho_{2,\text{F}_2} \in (\alpha_2, \alpha_3) \\
\rho_{3,\text{F}_1} &\in (\alpha_3, \alpha_4);
\end{aligned}$$

In actual GAMS implementation, we specify an absolute tolerance of 10^{-4} to bound the variables above (resp. below) from these lower (resp. upper) bounds.

5. Binary variables μ_i and their bounds:

$$\begin{aligned}
\mu_3^{\text{SEC}_2}, \mu_2^{\text{SEC}_3} &\in \{0, 1\} \\
\alpha_2\mu_3^{\text{SEC}_2} + \alpha_3(1 - \mu_3^{\text{SEC}_2}) &\leq \gamma_3^{\text{SEC}_2} \leq \alpha_3\mu_3^{\text{SEC}_2} + \alpha_4(1 - \mu_3^{\text{SEC}_2}) \\
\alpha_1\mu_2^{\text{SEC}_3} + \alpha_2(1 - \mu_2^{\text{SEC}_3}) &\leq \gamma_2^{\text{SEC}_3} \leq \alpha_2\mu_2^{\text{SEC}_3} + \alpha_3(1 - \mu_2^{\text{SEC}_3})
\end{aligned}$$

6. Feasibility constraints based on Equations (9) and (14):

$$\begin{aligned}
\gamma_3^{\text{SEC}_1} \geq \rho_{2,\text{F}_1} \geq \gamma_2^{\text{SEC}_2}; (1 - \mu_3^{\text{SEC}_2})(\gamma_4^{\text{SEC}_1} - \rho_{3,\text{F}_1}) &\geq 0; (1 - \mu_3^{\text{SEC}_2})(\rho_{3,\text{F}_1} - \gamma_3^{\text{SEC}_2}) \geq 0 \\
\mu_2^{\text{SEC}_3}(\gamma_2^{\text{SEC}_3} - \gamma_1^{\text{SEC}_2}) \geq 0; \gamma_3^{\text{SEC}_3} \geq \rho_{2,\text{W}_1} \geq \gamma_2^{\text{SEC}_2}; (1 - \mu_3^{\text{SEC}_2})(\gamma_4^{\text{SEC}_3} - \gamma_3^{\text{SEC}_2}) &\geq 0 \\
\mu_2^{\text{SEC}_3}(\gamma_2^{\text{SEC}_3} - \rho_{1,\text{F}_2}) \geq 0; \mu_2^{\text{SEC}_3}(\rho_{1,\text{F}_2} - \gamma_1^{\text{SEC}_4}) \geq 0; \gamma_3^{\text{SEC}_3} \geq \rho_{2,\text{F}_2} \geq \gamma_2^{\text{SEC}_4} &
\end{aligned}$$

Note that here, we only need to include constraints related to ρ_{2,W_1} , as the sidedraw stream contains only n-heptane and n-octane. Therefore, when implementing Equation (14) that involves ρ_{1,W_1} (resp. ρ_{3,W_1}), i.e., $\mu_2^{\text{SEC}_3}(\gamma_2^{\text{SEC}_3} - \rho_{1,\text{W}_1}) \geq 0$; $\mu_2^{\text{SEC}_3}(\rho_{1,\text{W}_1} - \gamma_1^{\text{SEC}_2}) \geq 0$ (resp. $(1 - \mu_3^{\text{SEC}_2})(\gamma_4^{\text{SEC}_3} - \rho_{3,\text{W}_1}) \geq 0$; $(1 - \mu_3^{\text{SEC}_2})(\rho_{3,\text{W}_1} - \gamma_3^{\text{SEC}_2}) \geq 0$), we add them to eliminate ρ_{1,W_1} (resp. ρ_{3,W_1}).

6. Additional constraints for sidedraw W_1 based on Equation (15):

$$\begin{aligned}
\gamma_2^{\text{SEC}_2} \leq \rho_{2,\text{W}_1}; \gamma_3^{\text{SEC}_3} \geq \rho_{2,\text{W}_1} \\
\mu_3^{\text{SEC}_2}(\gamma_3^{\text{SEC}_2} - \rho_{2,\text{W}_1}) \geq 0; (1 - \mu_2^{\text{SEC}_3})(\gamma_2^{\text{SEC}_3} - \rho_{2,\text{W}_1}) \leq 0
\end{aligned}$$

Here, we also only need to include constraints related to ρ_{2,W_1} .

Figure 13 below summarizes the relationships between μ_i and K_i variables for all column sections, which are used to write down the feasibility constraints and additional constraints based on Equations (9), (14) and (15) above.

	α_0	α_1	α_2	α_3	α_4	$\alpha_4 + \delta$
SEC ₁	$\mu_1 = 0$	$\mu_2 = 0$	$\mu_3 = 1$	$\mu_4 = 0$	$\mu_5 = 0$	
F ₁	$K_1 = 0$	$K_2 = 0$	$K_3 = 1$	$K_4 = 1$	$K_5 = 1$	
SEC ₂	$\mu_1 = 0$	$\mu_2 = 0$	$\mu_3 = ?$	$\mu_4 = ?$	$\mu_5 = 0$	
W ₁	$K_1 = 0$	$K_2 = 0$	$K_3 = ?$	$K_4 = 1$	$K_5 = 1$	
SEC ₃	$\mu_1 = 0$	$\mu_2 = ?$	$\mu_3 = ?$	$\mu_4 = 0$	$\mu_5 = 0$	
F ₂	$K_1 = 0$	$K_2 = ?$	$K_3 = 1$	$K_4 = 1$	$K_5 = 1$	
SEC ₄	$\mu_1 = 0$	$\mu_2 = 0$	$\mu_3 = 1$	$\mu_4 = 0$	$\mu_5 = 0$	
	$K_1 = 0$	$K_2 = 0$	$K_3 = 1$	$K_4 = 1$	$K_5 = 1$	

Figure 13: The relationships between μ_i and K_i variables for all column sections in the two-feed, one-(side)product column example discussed in Section 5.3 for quaternary separation. When the pinch root location for a specific column section is uncertain (labeled as “?” in the figure), it then needs to be defined as a binary variable μ_i . As shown in the constraints above, in actual implementation, we replace $\mu_4^{\text{SEC}_2}$ and $\mu_3^{\text{SEC}_3}$ with $1 - \mu_3^{\text{SEC}_2}$ and $1 - \mu_2^{\text{SEC}_3}$, respectively. The green arrows show how the (binary) coefficients present in the feasibility constraints of Equations (9) and (14) are constructed.